Best Practices for Multi-Point Ground Flares Design and Operation

Joseph Smith *, Jacques Dugué, Florian Euzenat, Ahti Suo-Anttila, Zach Smith, Vikram Sreedharan

Posted Date: 3 June 2026

doi: 10.20944/preprints202606.0243.v1

Keywords: CFD; multi-tip ground flare; thermal radiation; gas emissions; combustion; flare performance; flare regulations

 doi:10.20944/preprints202606.0243.v1

Article

Best Practices for Multi-Point Ground Flares

Joseph Smith [1,*], Jacques Dugué [2], Florian Euzenat [3], Ahti Suo-Anttila [4], Zach Smith [5] and Vikram Sreedharan [5]

[1] Chemical and Biochemical Engineering, Missouri Univ of Sci and Tech, Rolla, MO USA
[2] TOTAL, Direction industrielle /Equipements de Combustion et EnergieGonfreville, France
[3] TotalEnergies One Tech Gonfreville, Numeric DPP, France
[4] Computational Engineering Analysis LLC, Albuquerque, NM USA
[5] Elevated Analytics Consulting, St. Anthony, ID USA
* Correspondence: smithjose@mst.edu; Tel.: 1-918-760-1257

Abstract

Multi-Point Ground Flares (MPGF) are routinely used to process large quantities of flammable hydrocarbon gases. These flares use hundreds of flare burners arranged and fired in a staged configuration that increases the firing turn-down range. Wind fences that surround MPGFs shield flames from plant operators and nearby equipment. Safety concerns related to radiation flux, ignition cross lighting, and excessive emissions have been examined using Computational Fluid Dynamics (CFD) [1]. This paper examines the impact of MPGF burner and row spacing on flame radiation flux and the respective ground and fence temperature. It also examines flare ignition under windy and no-wind conditions and the effect this has on effluent dispersion during the ignition step. Validation of simulation results are presented to verify prediction accuracy. Based on this work, the following guidelines are proposed: 1. To improve flame height, flame shape, and smokeless performance, consider increasing row spacing. 2. To reduce soot formation and reduce flame height by increasing flame aeration, increase the porosity of the lower section of the wind fence. 3. Use air- and steam-assisted flare burners to increase MPGF combustion efficiency. 4. Using fewer flare tips with more flow area is more effective than using more tips with less flow area to reduce radiation flux to the ground and the wind fence which lowers surface temperature and reduces damage to the MPGF. 5. Using fewer large area flare tips that are optimally spaced increases combustion efficiency at full firing rate but lowers it at reduced firing rates during startup. 6. Wind fence designs that limit direct line-of-sight between flames and equipment outside the flare field reduce thermal damage to equipment located outside the wind fence. These recommendations are based on analysis results that illustrate how to successfully evaluate an MPGF design to ensure safe and clean operation for diverse firing scenarios.

Keywords: CFD; multi-tip ground flare; thermal radiation; gas emissions; combustion; flare performance; flare regulations

Introduction

Low profile Multi-Point Ground flares (MPGF) represent a special class of flares capable of safely processing (flaring) large quantities of flammable gas in an environmentally responsible fashion. Originally, these flares used "unstaged candle flares" and "pipe burners" (see Figure 1). Staged firing was developed and added in the early 1970's to broaden their turn down ratio and allow them to process larger gas flow rates (see Figure 2). Over the past 40 years, many improvements have been made to these large flares including: 1) optimizing the spacing be-tween burner tips to achieve efficient cross-lighting between burners in a row of burners from a single pilot located at the end of the burner row, 2) optimizing the space between adjacent rows of burners to allow for sufficient air to support complete combustion above burners located in the middle of the burner row, 3)

 doi:10.20944/preprints202606.0243.v1

development of advanced wind-fence design to allow adequate air to enter the flare field while protecting equipment and personnel outside the flare field from flame radiation, 4) use of air and steam assist media to support low pressure operation, and 5) advanced burner tip design to enhance combustion efficiency. Of particular importance is the use of "staging" the flow rate to facilitate a large turn down ratio while maintaining highly efficient smokeless combustion of a MPGF.

Figure 1. Early Multi-Point Ground Flare designs circa 1950-2000 (courtesy Zeeco, Inc.).

Figure 2. Early MPGF in Beaumont, Texas circa 1960 (courtesy Zeeco, Inc.).

This paper presents a brief history of MPGF development. It also analyzes the performance of a specific MPGF burning flare gas with varying amounts of hydrogen and ethylene during startup and emergency relief firing conditions . Specific questions regarding MPGF operation and design are addressed in this paper including:

1. What impact does using fewer large flare tips (more flow areas = higher flow rate per burner) compared to using more small flare tips (less flow area = lower flow rate per burner) on flame height and flare performance?
2. What impact does extra space between adjacent rows of burners have on combustion efficiency and radiation to the fence and ground?
3. What impact does assist media (steam or air) have on flare performance?
4. How does high hydrogen concentration impact flame radiation to the fence and ground?
5. How does high ethylene concentration impact flame radiation to the fence and ground?

An advanced Large-Eddy Simulation (LES) based computational fluid dynamics (CFD) model is used to analyze transient behavior for the MPGF for base load firing conditions. Various design conditions are then evaluated. Finally, results from the base load cases and the design cases are used to optimize the MPGF design.

Historical Perspective of Multi-Point Ground Flares

 doi:10.20944/preprints202606.0243.v1

To illustrate how MPGF design has evolved over time, a modern MPGF (see Figure 3) shows multiple stages, row spacing, and a small wind fence located away from the burners to prevent thermal damage to the fence.

Figure 3. Multi-Point Ground flares built and operated as part of a petroleum production (courtesy Zeeco, Inc.).

Improvements in MPGF design have addressed several important issues including:

1. Ability to fire non-standard flow rates over longer periods safely,
2. Clean combustion for non-standard flaring scenarios for varied flare gas composition over a wider range of tip pressures and gas temperatures,
3. Relative spacing between flare field and nearby equipment and personnel for design and non-design flow rates with associated radiation flux from the flame,
4. Wind fence design efficiently protects equipment and personnel from flame radiation,
5. Wind fence design that allows sufficient air to promote clean efficient combustion for standard and non-standard gas composition, operating pressure/ temperature and external wind,
6. Noise emissions from operating flares and their impact on workers and the surrounding community, and
7. Flare burner tip design to promote local air/fuel mixing to support clean, efficient combustion.

Today's MPGFs use engineered flare burner tips that promote efficient air/fuel mixing to enhance combustion efficiency (see Figure 4). These tips employ variable area arms made of 310 SS using investment casting and are pressure tested for safe operation. Extensive fuel staging maintains high destruction efficiency over a wide range of flare gas flow rates (see Figure 5). Of particular focus is clean operation at low flow rates where air/fuel mixing is difficult due to a lack of mixing energy. MPGFs also include a wind fence to shield surrounding equipment and personal from flame radiation while allowing sufficient air to enter the flare field required for high destruction efficiency. Wind fences are optimized to reduce the steel required for fabrication of high structural integrity required to withstand stresses caused by high winds. Finally, the wind fence is designed to protect flare flames from cross winds effects (see Figure 6).

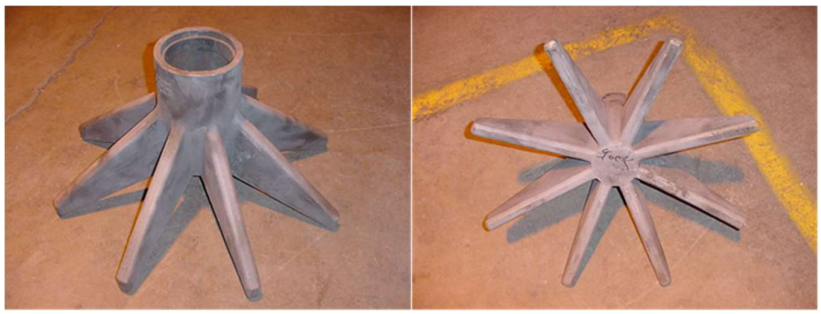

Figure 4. Flare tips used in MPGF systems ensure proper air/ flare gas mixing (courtesy Zeeco, Inc.) [2].

 doi:10.20944/preprints202606.0243.v1

Figure 5. Modern ground flare system includes complex piping systems to stage flare gas to accommodate wider operating ranges with high combustion efficiency (courtesy Zeeco, Inc.) [2].

Figure 6. Effective wind fence designs protect surrounding equipment and personnel from high radiation flux while providing necessary air for efficient combustion (courtesy Zeeco, Inc.) [2].

Safety issues related to ignition of an MPGF at a large gas processing plant in Norway have been discussed earlier by Smith et al. [3,4]. Tip and row spacing that allow effective cross lighting has been studied and optimized by vendor testing which depends on the specific flare burner design specific to a vendor's flare design and operation as illustrated by a MPGF designed by Zeeco (see Figure 7).

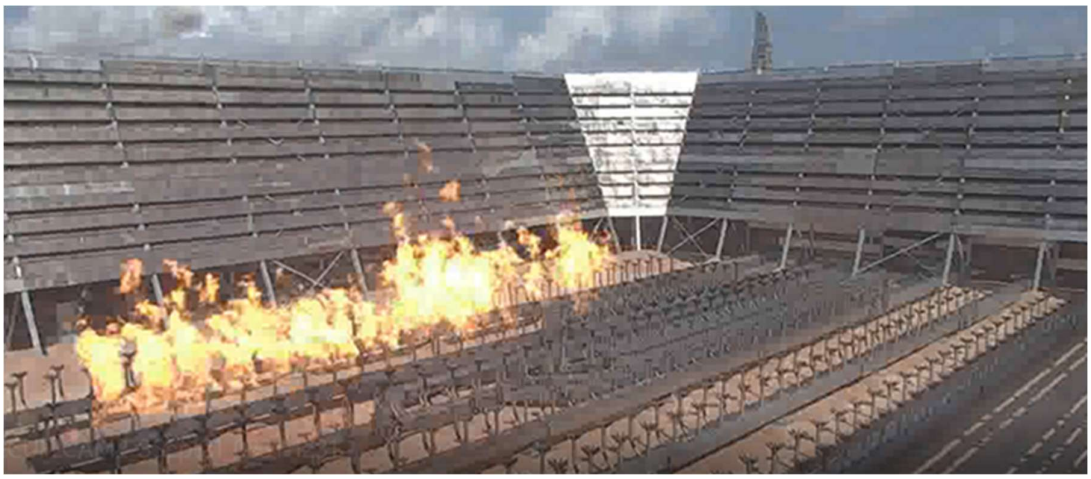

Figure 7. MPGF located in Port Arthur Texas, USA, stages 1 and 2 burning (courtesy Zeeco, Inc.) [5].

Given the development history and background of MPGF, the remainder of this paper will focus on a detailed analysis of a modern MPGF which provides information used to establish the recommended design criteria and recommended operating limits for a MPGF.

MPGF Analysis

 doi:10.20944/preprints202606.0243.v1

A detailed computational fluid dynamics (CFD) model of a low-profile MPGF (Figure 8) has been developed using the flare modeling tool called *C3d*. This CFD tool has been used to simulate many flare systems including enclosed flares, elevated steam and air-assisted flares, pressure-assisted flares, and MPGFs. This MPGF system is located in Port Arthur, Texas in the gulf coast region of the United States. As shown, the MPGF is positioned on top of an elevated embankment, above ground level. The MPGF flare field was 172 ft (52.4 m) wide and 224 ft (68.3 m) long surrounded by a 50 ft (15.2 m) high wind fence to shield the flames from the normal 10 mph (30 km/h) wind blowing from the south across the flare field (see Figure 9).

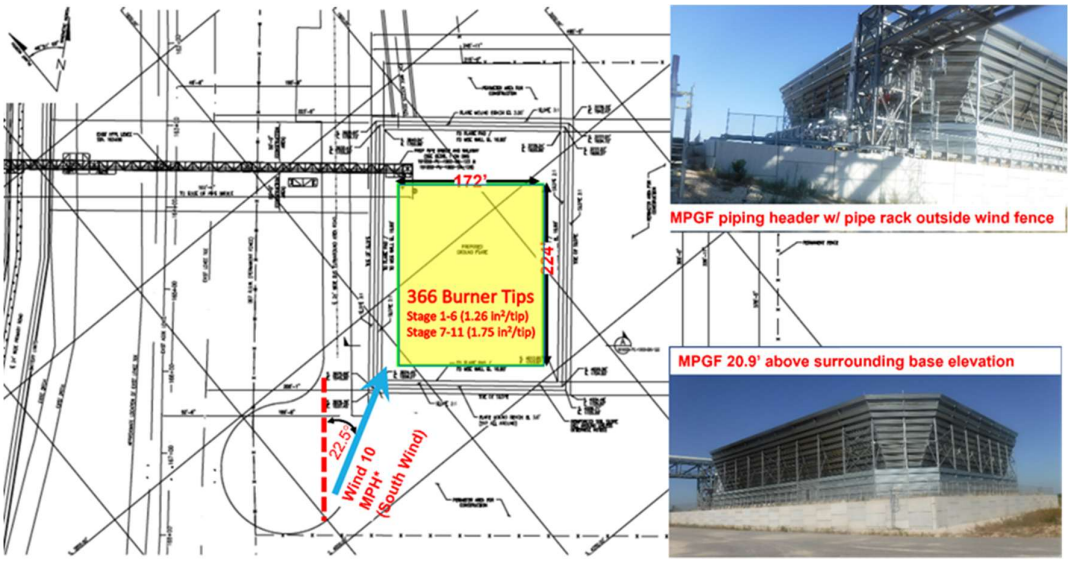

Figure 8. Port Arthur MPGF with 366 flare burners in 10mph south wind (Emergency Firing High Ethylene Flare Gas: 94.0 mol% C2H4, 6.0 mol% C2H6, Mol Wt 28; Startup Firing High Hydrogen Flare Gas: 34.5 mol% C2H4, 23.1 mol% C2H6, 33.1 mol% H2, 5.7 mol% CH4, 0.60 mol% C3H6, Mwt 19.4).

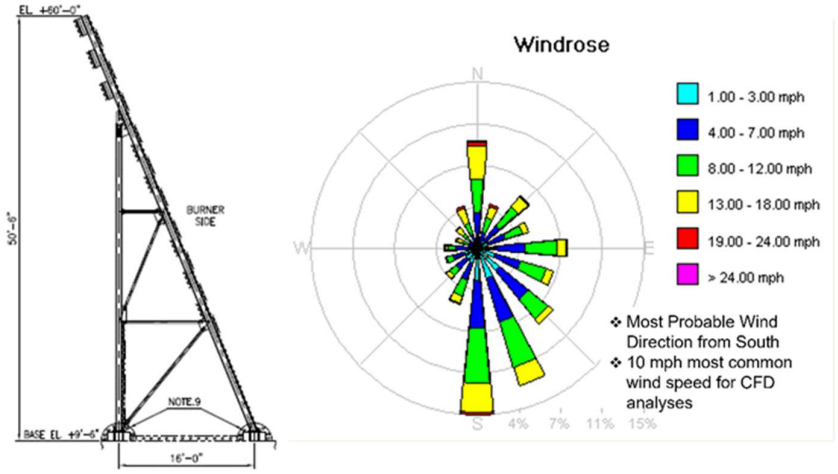

Figure 9. Total MPGF Wind fence and prevailing wind data.

Previous code validation work was performed [6,7] to evaluate the combustion model used to analyze the complex turbulent reacting flow chemistry occurring in hydrocarbon combustion inherent in MPGF operation [8–10].

The work described in this paper focuses on CFD analysis to evaluate the impact of various design features and operating conditions on MPGF performance. Results of 30 different CFD cases

 doi:10.20944/preprints202606.0243.v1

that examined to assess how tip and row spacing, tip size, steam assist and fence design affects flare operation. Flare performance was quantified using various metrics including:

1. Percent radiation loss from the flame,
2. Soot and CO Iso-surfaces colored by temperature,
3. Flare Destruction Efficiency, and
4. Fence and Ground Temperature.

Based on this work, general design and operating recommendations were developed and are presented in this paper. This work is intended to provide a guide for vendors and end-users to improve safe and efficient flare operation. Although the results presented in this paper are for a specific MPGF, results and conclusions are applicable for general MPGF design and operation.

Modeling Multi-Point Ground Flares

The CFD tool used in this work simulates hydrocarbon combustion coupled with radiative heat transport from a large flare to nearby objects including wind fences, piping manifolds, pipe runner and adjacent burner tips. The code can be used to provide a "reasonable" estimate of common risk scenarios including flame impingement due to cross winds, low combustion efficiency, thermal fatigue of wind fences, pipe runners and racks, and other surrounding equipment, and high heat exposure for operating personnel, for a given flare design and flare gas composition and flow rate.

Typical simulations generally require CPU times on the order of hours to a few days using a "standard" windows (or LINUX) desktop workstation. Large Eddy Simulation (LES) is used to approximate transient mixing. The flare CFD tool is called *C3d* which is specifically tailored to analyze large gas flare performance. *C3d* has previously been applied to large multipoint ground flares, air- and steam-assisted flares, and utility flares [8]. Various combustion models have been developed, implemented, and tested for various flare gas compositions including methane, ethane, ethylene, propane, propylene and xylene [7]. *C3d* has been used to predict flare flame size and shape, estimate the smoking potential for a given flare design firing typical flare gas, and to estimate radiation flux from the flare flame to surrounding surfaces. Transient simulations of flame height and flame-to-ground radiation have been validated by comparison to measured flame size, shape, and radiation measurements taken during single-burner and multi-burner tests conducted under no-wind and low-wind ambient conditions [9].

For the MPGF considered in this work, *C3d* simulations were performed for start-up and emergency relief firing conditions subject to a crosswind blowing across the flare field. The impact of row spacing and tip spacing was examined along with burner flow area (tip size) and steam and air assist media. Multiple wind fence designs were examined to assess the impact of air flow through the base of the flare compared to flow into the main flame region. Predictions of maximum ground and fence surface temperature were recorded for various flare designs. The expected flare destruction efficiency (DRE) and the amount of flame radiation lost to nearby surrounding was examined for each scenario case examined.

Technical Approach

Due to the size of a typical MPGF, modeling the exact fence geometry was not practical since it would require an excessive number of computational cells and the associated CPU time to perform a fully transient LES CFD analyses of the MPGF. Instead, a previously developed methodology to approximate the fence design and multi-port flare burner was used to approximate the actual MPGF geometry [8].

A "structured" computational grid composed of hexahedral cells (see Figure 10) was used in the simulations. The total height of the computational domain was increased to avoid any effect caused by the top boundary that might impact predicted flame height and/or plume dispersion downwind of the flare. A mesh independence study was conducted using several different meshes to confirm mesh independent results. A typical mesh independence study is routine for standard steady-state

 doi:10.20944/preprints202606.0243.v1

RANS based CFD analysis, this type of analysis is much harder to implement and interpret for transient LES CFD analyses due to the time-varying nature of LES solutions. Furthermore, results in a mesh sensitivity study of a large MPGF includes many coupled effects complicated by transient non-uniform wind profiles. For the current work, the *C3d* model of the MPGF flame was tuned using results from earlier validation cases. This required the full MPGF case to use a similar sized mesh as the validation cases. These criteria set the relative cell size and resulting mesh density used in this work. Based on the mesh study, the final computational mesh for the MPGF flare consisted of 3.34 million cells with mesh refinement near the flare burners.

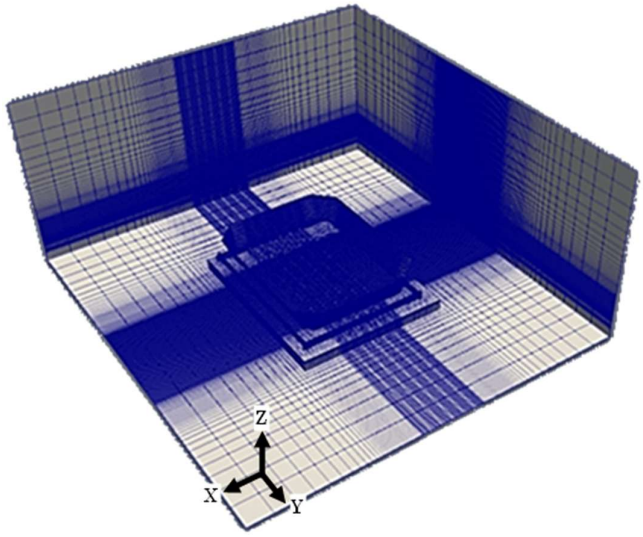

Figure 10. Hexahedral mesh (3.34 million cells) used for multi-zone analysis of flame shape and radiation flux. Domain extended 230ft (70m) above flare to avoid upper boundary effect.

Combustion Model

Turbulent combustion reaction kinetics can be simulated using a single step in the CFD model. The stoichiometric coefficients and reaction rate constants are fit to measured rate data. Although one simulation might use the same global reaction mechanism and rate coefficients published for another simulation, this often produces incorrect results since the published mechanism and associated rate coefficients have been developed and tuned for a specific data set for a combustion experiment. In general, simulation results are sensitive to the computational mesh (cell size, aspect ratio, number of cells) and the kinetic data used to build a simplified combustion model. Applying a specific combustion model to a new simulation of a different application using a different mesh requires a different set of reaction coefficients. To accurately simulate a MPGF, a consistent set of chemical reactions describing hydrocarbon combustion is required. To minimize the computational load, a reduced number of chemical reactions must be used to approximate the total energy generated by the reactions along with the species consumed and produced. To accurately simulate the combustion chemistry in a MPGF flame, details of the chemical reactions are not critical if the oxygen consumption is correctly balanced for the fuel type and the soot produced is properly calibrated with experimental data.

For systems burning complex hydrocarbon mixtures, a combustion model covering a wide range of fuels and intermediate species has been developed and validated [7]. This model separates combustion into primary fuel breakdown reactions which form intermediate species followed by combustion of those intermediate species.

Primary fuel breakdown reactions for a wide range of hydrocarbon fuels include:

$1.5C_2H_4 + 1.5O_2 \rightarrow CO + C_2H_2 + 2H_2O$ *Ethylene breakdown* (1)

 doi:10.20944/preprints202606.0243.v1

$C_3H_8 + 1.5O_2 \rightarrow C_2H_2 + 2H_2O + CO + H_2$	*Propane breakdown*	(2)
$C_2H_6 + 0.5O_2 \rightarrow 0.5C_2H_2 + CO + H_2$	*Ethane breakdown*	(3)
$C_3H_4 + O_2 \rightarrow C_2H_2 + H_2O + CO$	*Propadiene breakdown*	(4)
$C_5H_{12} + 4O_2 \rightarrow C_2H_2 + 5H_2O + 3CO$	*N-Pentane breakdown*	(5)
$C_4H_6 + 4O_2 \rightarrow 2C_2H_2 + H_2O$	*1,2, Butadiene breakdown*	(6)
$C_3H_6 + 1.5O_2 \rightarrow C_2H_2 + 2\,H_2O + CO$	*Propylene breakdown*	(7)
$C_{12}H_{26} + 6.5O_2 \rightarrow 7H_2O + 2CH_4 + 2C_2H_2 + 6CO$	*Dodecane breakdown*	(8)

These reactions can be used individually or combined into a single fuel breakdown reaction for a gas mixture by applying the respective mole fractions of each component and adding the mole fraction weighted reactions-terms together to form a single fuel breakdown reaction for the mixed fuel. For example, combustion of a flare gas composed of ethylene and propylene could be approximated by combing the individual breakdown reactions for ethylene (Eq.1) and propylene (Eq. 7) using the appropriate mole fractions of each species in the gas mixture.

For more complex hydrocarbon mixtures, the fuel is approximated by breaking down the complex hydrocarbon into CO, C_2H_2, H_2 and H_2O with stoichiometric coefficients estimated using three rules:

1. Heavy sooting hydrocarbons produce more C_2H_2 and possibly a small amount of soot,
2. Heat release for primary fuel breakdown should be adjusted by producing more H_2O for higher heat release or more H_2 for less heat release, and
3. The oxygen consumption balance, and associated CO production should be determined by an elemental balance.

Testing this approach showed that the combustion model based on methane combustion has mild sensitivity to the primary breakdown reactions, which allows flexibility in developing advanced combustion models for mixed flare gases. Testing the combustion model with a variety of different flame/flare simulations showed that secondary reactions are mostly determined by the flame temperature and soot production.

$H_2 + 0.5O_2 \rightarrow H_2O$	*Hydrogen combustion*	(9)
$C_2H_2 + 0.9O_2 \rightarrow 1.8CO + H_2 + 0.01C_{20\,(soot)}$	*Acetylene combustion/ soot nucleation*	(10)
$C_2H_2 + 0.01C_{20\,(soot)} \rightarrow H_2 + 0.11C_{20\,(soot)}$	*Acetylene/soot combustion/ soot growth*	(11)
$CO + 0.5O_2 \rightarrow CO_2$	*CO combustion*	(12)
$C_{20\,(soot)} + 10O_2 \rightarrow 20CO$	*Soot combustion*	(13)
$CH_4 + 0.5O_2 \rightarrow 2H_2 + CO$	*Methane combustion*	(14)
$C_2H_2 + 3H_2 \rightarrow 2CH_4$	*Forward Acetylene-Hydrogen-Methane Equilibrium*	(15)
$2CH_4 \rightarrow C_2H_2 + 3H2$	*Reverse Acetylene-Hydrogen-Methane Equilibrium*	(16)
$C_2H_4 + H_2O \rightarrow CO + 0.5C_2H_2 + 0.5H_2$	*Ethylene – Water Reforming*	(17)
$C_{20\,(soot)} + 20H_2O \rightarrow 20CO + 20H_2$	*Soot – Water Reforming*	(18)

An advantage of using this approach is that the initial reaction for burning the flare gas has a low value of activation energy, which allows partial burning and heat release from flare gas combustion. This maintains stable combustion since the partial heat released supports the subsequent reactions, which produce most of the heat and all the soot in the flame.

Similar to previous combustion models developed and used to analyze MPGFs [3,8], the flare gas Arrhenius combustion time scale is combined with the turbulence eddy breakup time scale to yield an overall time scale for each reaction rate:

$$t_{total} = t_{arrhenius} + t_{turb} = \frac{1}{C_i} = \frac{1}{A_k T^b exp^{-\left(\frac{T_A}{T}\right)}} + \frac{C_{eb}\Delta x^2}{\varepsilon_{diff}} \quad (19)$$

where A_k is the pre-exponential coefficient, T_A is an activation temperature, T is the local gas temperature, and b is a global exponent, Δx is the characteristic cell size, C_{eb} is a user input constant (~0.2E-04) that is cell size dependent, ε_{diff} is the eddy diffusivity from the turbulence model, and t_{turb} is the turbulence time scale (characteristic time required to mix contents in a computational cell). The reaction rates are combined by simple addition of the time scales. Depending on the scale of the Arrhenius verses the turbulent time scales, the characteristic time for each reaction can be different.

 doi:10.20944/preprints202606.0243.v1

Thus, the combustion model approximates turbulent combustion using the Eddy Dissipation Concept (EDC) and local equivalence ratio effects. The Arrhenius kinetics and turbulent mixing approach are similar to the more commonly used Eddy-Breakup (EBU) combustion model.

To this end, a multi-step chemical reaction model was developed using breakdown reactions (Eqs. 1-8) and the secondary combustion reactions (Eqs. 9-18) for the flare gas burned in the MPGF. All rate equations are solved simultaneously for each reaction, and the stoichiometric coefficients are used as constraints that couple the equations and ensure conservation of energy and chemical species.

In the present work, the global reaction mechanism described by Suo-Anttila [7] was used. Suo-Anttila's work relied on previous work by Duterque et al. [11] and Kim and Maruts [12] as starting points. However, since these authors adjusted their global reaction coefficients to match "laminar" flame speed and since combustion occurring in a MPGF flame is governed by turbulent mixing, the original coefficients had limited applicability. The coefficients associated with the activation temperature and the exponents for mole fractions based on the reaction mechanism physics were not expected to be affected by local grid structure. However, this turned out not to be the case for the pre-exponential coefficients. To match reaction rates to measured combustion rates, the pre-exponential coefficients for all reactions were adjusted to provide a validated combustion model. Also, since the combustion model depended upon turbulent flare gas mixing, combustion was also expected to be governed by turbulent mixing with ambient air. The *C3d* code uses an LES formulation to approximate turbulent mixing, which depends upon two additional factors, a proportionality coefficient and cell size. The recommended LES proportionality coefficient of 0.15 was used. To capture the cell size dependency correctly, the same computational mesh characteristic dimensions were used in the full MPGF mesh as used in the triple ethylene flare radiation validation test (see Figure 11) and the earlier single flare tip test (see Figure 12). With this information, the required kinetic parameters listed in Table 1 were established for the validated combustion model required in the present simulations.

Figure 11. Comparison of Predicted and Measured Flame Shape for 3-Flare Test (sequential predicted images overlaid recorded flame image) [13].

 doi:10.20944/preprints202606.0243.v1

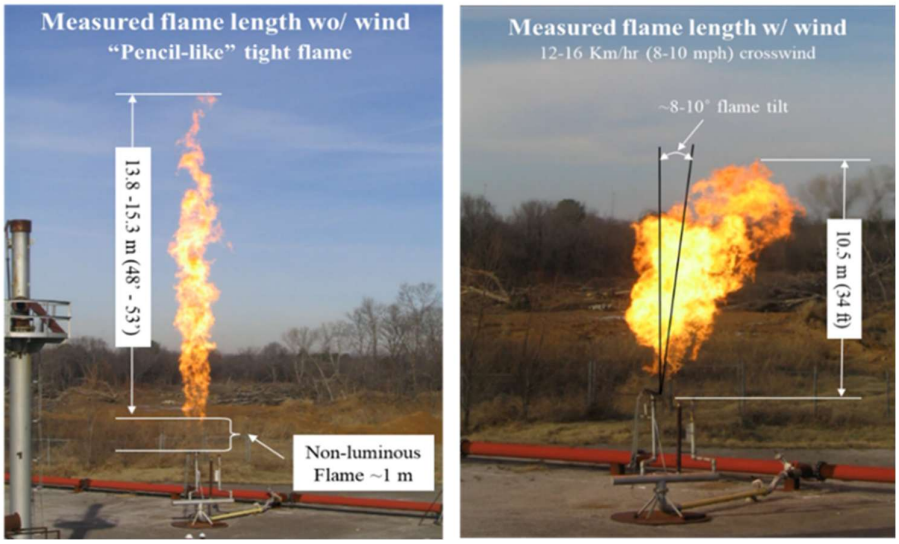

Figure 12. Wind effects on the flame shape of single flare tip with propane flow rate: measured at 1.4 in-wc @ 57 °F across orifice plate (7.3 psig tip pressure on 0.457m pipe) [8].

Table 1. Reaction parameters used in MPGF combustion model.

Reaction	f_1	f_2	T_A (K)	C (1/s)	B
Primary Fuel Breakdown (ethylene)	$[C_2H_4]^{0.1}$	$[O_2]^{1.65}$	0 K	1	2
Hydrogen Combustion	$[H_2]^{0.33}$	O_2	10000 K	1e8	0
Acetylene combustion & soot nucleation	$[C_2H_2]^{0.33}$	O_2	15110 K	2e8	2
Acetylene + soot growth	$[C_{20}]^{0.33}$	C_2H_2	15110 K	1e7	0
CO – Oxygen combustion	CO	$[O_2]^{0.25}[H_2O]^{0.5}$	20142 K	1e18	0
Soot combustion	$[C_{20}]^{0.33}$	O_2	0 K	0.5	0.75
Methane combustion	CH_4	O_2	15000 K	1e12	0
Forward Acetylene – Hydrogen – Methane	C_2H_2	H_2	15110 K	5e7	0
Reverse Acetylene – Hydrogen - Methane	CH_4	CH_4	23500 K	4e9	0
Ethylene - Water Reforming	C_2H_4	H_2O	15000 K	5e6	0
Soot – Water Reforming	$[C_{20}]^{0.1}$	$[H_2O]^{1.7}$	0 K	1.0	0.75

Modeling Assumptions

The following modeling assumptions were used in this work:

1. Combustion of the flare gas was approximated by the chemical reaction mechanism described above using the specified kinetic coefficients (see Table 1).
2. Thermal radiation was calculated using the standard *C3d* radiation model.
3. Ambient wind condition, inlet flare gas temperature and pressure, were set to match the specified operating conditions.

Boundary Conditions

The Boundary conditions employed in the *C3d* simulations included an imposed wind speed on the upwind side of the computational domain with hydrostatic pressure boundaries proscribed over all other sides except the ground where a zero mass-flux boundary was imposed. The thermal and species boundary conditions were set for each case, assuming standard air composition with ambient air temperature as 73°F (23°C).

 doi:10.20944/preprints202606.0243.v1

Physical and Numerical Sub-Models

As stated earlier, *C3d* uses a standard LES formulation to approximate the turbulent mixing. The governing equations for this LES based CFD tool, assuming incompressible fluid flow, are given below. [14]

The steady-state continuity equation is:

$$\partial(\rho u_i)/\partial x_j = 0 \quad (20)$$

where ϱ is the density of the gas (mixture) and u is the three-dimensional velocity vector.

The momentum equation is:

$$\partial(\rho u_i u_i)/\partial x_j = \partial P/\partial x_i + \partial \tau_{ij}/\partial x_j + \rho f_i \quad (21)$$

with f_i as the body forces, P as the pressure, and τ_{ij} represented as the stress defined as:

$$\tau_{ij} = \mu\left(\partial u_i/\partial x_j + \partial u_j/\partial x_i\right) + (\mu_B - 2/3\,\mu)\,\partial u_k/\partial x_k \delta_{ij} \quad (22)$$

The other governing equation solved in C3d is the energy equation:

$$\rho\, c_p\ \partial(T)/\partial x_j = -(\nabla . q) - \left(\frac{\partial \ln \rho}{\partial \ln T}\right)\frac{Dp}{Dt} - (\tau : \nabla v) \quad (23)$$

where C_P is the specific heat. The energy equation is used to capture the temperature changes due to combustion and mixing. The energy equation also includes radiation effects.

To resolve sub-filter scales for LES turbulence model, the Gaussian filter is used as shown in equation:

$$G(x - r) = [\![(6/(\pi \Delta \hat{}\, 2\,))]\!] \hat{}\, (1/2)\ \exp\left(-(6(x - r)\hat{}\, 2)/\Delta \hat{}\, 2\,\right) \quad (24)$$

The following equations are used to simulate the kinetic energy dissipation on subgrid scales to molecular diffusion:

$$\tau_{ij}^r - 1/3\,\tau_{kk}\delta_{ij} = -2\nu_t \bar{S}_{ij} \quad (25)$$

$$\bar{S}_{ij} = 1/2\,\left(\frac{\partial \bar{u}_i}{\partial x_j} + \frac{\partial \bar{u}_j}{\partial x_i}\right) \quad (26)$$

with τ_{ij}^r as the stress tensor, $\bar{S}_{ij}$ as the rate-of-strain tensor, and ν_t as the turbulent eddy viscosity. The eddy viscosity is approximated as the characteristic length scale times the velocity scale in the subgrid scale model as implemented in the Smagorinsky-Lilly model:

$$\nu_t = (C_s \Delta_g)^2 \sqrt{2\bar{S}_{ij}\bar{S}_{ij}} = ((C_s \Delta_g)^2 |S|, \qquad C_s = \text{Constant}, \qquad \Delta_g = \text{grid size}$$

The equilibrium assumption was applied between energy production and dissipation of small scales in this model.

The multi species conversation equations form is shown in equation (14)

$$\frac{\partial \rho m_i}{\partial t} + \nabla . \rho V m_i = -\nabla . \vec{J}_i + R_i + S_i \quad (27)$$

where, m_i is the mass fraction of species i, $\vec{J}_i$ is the diffusion flux of species i, R_i is the mass creation or depletion by chemical reactions, and S_i mass source. The species equations are solved to keep track of the distribution and concentration of fuel, oxygen, intermediate species, soot, and products of combustion (CO_2 and H_2O). The combustion model was used to provide the species equations source and sink terms as a function of species concentrations, local gas temperature, and turbulent diffusivity.

C3d also includes sub-models to predict flame emissivity as a function of molecular gas composition, soot volume fraction, flame size, shape, and temperature distribution which in turn depend on solutions to the mass, momentum, energy, and species transport equations. The radiation transport model predicts radiation flux on external (and internal) surfaces, as well as provides the source and sink terms for the energy transport equation (Eq. 23) so that the flame temperature distribution can be accurately predicted.

Thermal radiation effects in *C3d* are calculated in two ways. Within the flame zone, radiation is assumed to be diffusive and outside the flame zone radiative transport is calculated using view-factor methods. The flame surface used in the view-factor calculation is set by finding the dynamic surface wherein a product of hydrocarbon combustion, typically carbon dioxide, has a mass fraction above and below a user-specified value, typically 0.04. This dynamic surface, its temperature, and a

 doi:10.20944/preprints202606.0243.v1

correction factor (dependent upon flame optical thickness) are all used to calculate view-factor radiation from all flame surfaces to surrounding objects including nearby process instruments, equipment, and structures to identify safe work zones. The view-factor radiation calculation also includes shadowing due to intervening objects. It also includes radiation absorption along the ray path due to "participating" media such as water vapor, carbon dioxide, and soot. Finally, it includes absorption and re-radiation from the ground.

The view-factor radiation calculation has also been implemented in a multi-zone version of *C3d* to allow multi-Block meshes required for large systems including multiple MPGF systems. The multi-block formulation allows the user to split a large problem into separate zones which are coupled together at the boundary conditions. Each zone is solved on a different CPU with time synchronized so large problems requiring 10's to 100's of millions of cells can be solved on multiple CPU's simultaneously to reduce overall computational time. The view-factor thermal radiation from one block (or zone) can be calculated to any geometric position either within or outside that zone. This allows the user to add radiation contributions from adjacent zones to get the total incident radiation value for the entire problem. The only restriction in this zone-to-zone radiation transport method is related to shadowing and media absorption in adjacent zones which is not considered because adjacent zones only know about geometric and compositional details within the zone boundaries.

Radiation Validation

Predicting heat transfer from the flare flame depends not only on accurate simulation of the combustion chemistry which relates to flame size and shape but also to how heat is transferred from the flame to the surrounding. Most energy from a large MPGF flame leaves with the heated plume but a fraction of it is lost from the flame via radiative heat transfer to the surrounding wind fence and ground surfaces. Therefore, the radiation model used in *C3d*, discussed earlier by Smith et al. [8,15], was re-examined and validated by comparing predicted radiation heat loss from a multi-burner flare flame and predicted values from a *C3d* simulation.

Previous radiation validation studies (see Figure 13) were conducted using a propylene fuel fired through nozzle tips similar to that shown in Figure 14. This flare burner tip had a 2-in^2 flow area commonly used for MPGFs. In this test a single tip was used with 5.5 kg/sec propylene injected at 22.5 PSIG. During the test, the flare was fired into a 3-7 MPH (10.3 – 25.2 km/h) crosswind gusting to 9-13 MPH (32.4 -46.8 km/h). Radiation flux measurements were taken at three distances from the flame: 75 ft (22.9m), 100 ft (30.48m), and 150 ft (45.7m), and at two elevations - 5 ft (1.5m) and 20 ft (6m) elevations. The radiometers were placed due east of the flare with the wind blowing from South Southeast 169 degrees from true north.

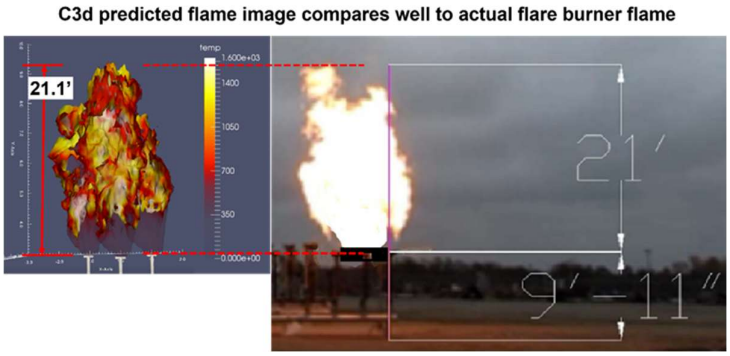

Figure 13. C3d radiation validation using 3 flare burner test firing propylene.

 doi:10.20944/preprints202606.0243.v1

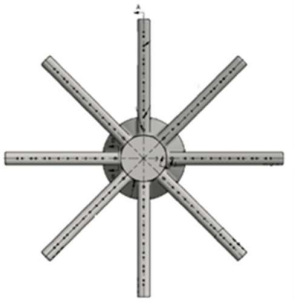

Figure 14. Flare burner tip used in validation tests (courtesy Zeeco, Inc.).

Two simulations were performed considering 5 mph (8km/h) and 10 mph (16km/h) wind speeds. Flare radiation is very sensitivity to wind speed. Previous work compared a flare flame standing straight up under no wind to a shorter bushier flame deflected downwind under windy conditions [8]. The wind speeds considered in the validation simulations considered two speeds that also covered wind gusts encountered during the flare test. Simulations also considered atmospheric absorption due to CO_2 and H_2O utilizing the Fuss and Hamins correlation [16].

The *C3d* simulation domain included a 12 m x 12m (39.4 ft x 39.4 ft) square computational domain 20m high (65ft) with a variable grid composed of 328,000 cells. This simulation required approximately 4 CPU hours from ignition to steady state operation on a standard desktop computer. As shown in Table 2, all measured results are within the predicted band limited by the two wind speeds. This work reaffirmed the sensitivity of flare radiation to wind speed as originally discussed by Smith et al. 2007 [8].

Table 2. Predicted verses measured radiation fluxes at 6 locations for 2 wind speeds.

Elevation (wind speed) Sample distance from flare	5 ft high (3-7mph measured wind) Measured Flux (BTU/hr-ft²)	5 ft high (5mph predicted wind) Predicted Flux (BTU/hr-ft²)	5 ft high (10mph predicted wind) Predicted Flux (BTU/hr-ft²)	20 ft high (3-7mph measured wind) Measured Flux (BTU/hr-ft²)	20 ft high (5mph predicted wind) Predicted Flux (BTU/hr-ft²)	20 ft high (10mph predicted wind) Predicted Flux (BTU/hr-ft²)
75 feet	171	190	168	205	221	183
100 feet	102	117	95	102	120	104
150 feet	34	53	38	34	53	38

CFD Analysis and Results

To evaluate the MPGF using CFD, a base design for the specific unit was selected. An approximation of the burner rows and row spacing with staging sequence and numbers of flare tips per row in each stage and relative size of each flare tip was used in base case analyses (see Figure 15).

 doi:10.20944/preprints202606.0243.v1

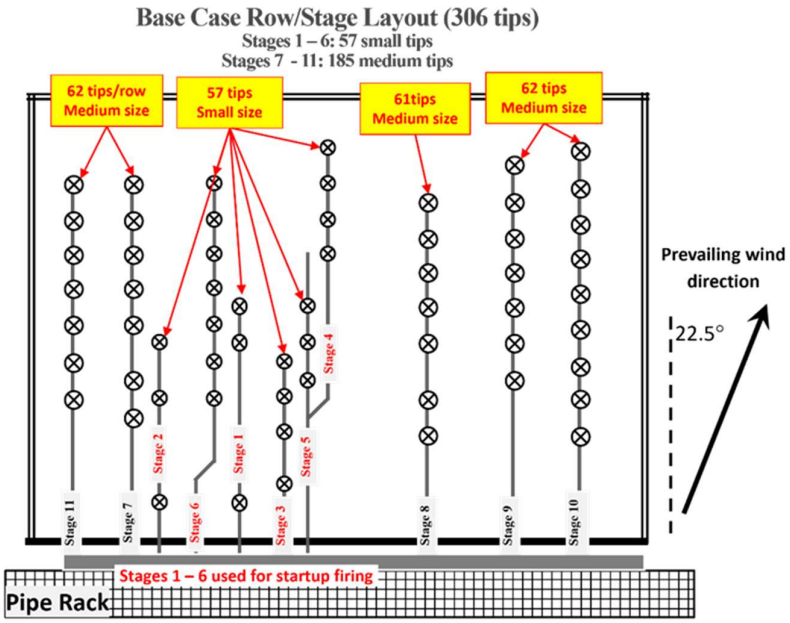

Figure 15. Base MPGF configuration showing burner rows and flow staging with relative numbers and size of flare tips used in each stage[1].

During the CFD analysis of this specific operating MPGF, 20 CFD cases were conducted which simulated the "Base Design" (Table 3), an evaluation of various design options (Table 4) and several cases with the design options combined and case results evaluated to optimize the MPGF design (Table 9). To analyze and compare results from all of these CFD cases, a list of metrics was developed to quantify flare performance as a function of design features (i.e., tip flow area, runner spacing, fence open area, etc.) and operating parameters (i.e., flare gas composition, flare gas flow rate, etc.). These metrics are listed below:

1. Soot based opacity iso-surface colored by temperature,
2. O2 iso-surface colored by velocity magnitude,
3. Air supplied to flare burners compared to expected air demand,
4. Flare destruction efficiency (DRE),
5. Iso-surface of unburned flare gas colored by temperature,
6. Iso-surface of 0.05 ppm soot concentration colored by temperature,
7. 2,000 ppm CO iso surface colored by elevation above grade,
8. 2,000 ppm CO iso-surface times carbon count of the fuel colored by elevation above grade,
9. Fence surface temperature (K) with x, y, z coordinates of peak fence temperature,
10. Ground surface temperature (K) with x, y, z coordinates of peak ground temperature,
11. Fence radiation flux (W/m2) with x, y, z coordinates of peak flux to the fence,
12. Percent Radiation loss from the Flame,
13. Wind streamlines showing impact of wind on burner performance,
14. Ground incident radiation (W/m2) showing location of peak radiation to ground, and
15. Reverse streamlines from the flame surface.

Table 3. Base design CFD Case Descriptions.

[1] Note: Configuration shown only give relative burner/row orientations and do not represent design drawings

 doi:10.20944/preprints202606.0243.v1

Case Name (running case #)	Case Description
C1 (Base Case 1)	Full firing of high ethylene flare gas through stages 1-6 with 59 small sized tips and stages 7-11 with 185 medium sized tip, normal tip elevation with open lower fence with 10mph south wind. Worse case scenario.
C2 (Base Case 2)	Startup firing rate of high ethylene flare gas with stages 1-6 firing 120 small sized tips and stages 7-11 firing 185 medium sized tip, normal tip elevation with open lower fence in a 10mph south wind. One runner startup scenario.
C3 (Base Case 3)	Startup firing rate of high hydrogen flare gas through stages 1-8 with 120 small tips on two runners, normal tip elevation with open lower fence with 10mph south wind. Two runner startup scenario.

Table 4. CFD input for Base Cases 1 - 3.

Case C1 (Base Case 1) Model Input

Parameter	Value	Flare Gas	Value
Ambient Temperature	95°F	MW	28.2
Ambient Pressure	14.7 psia	L.H.V.	1,508 BTU/SCF
Wind Speed	10 MPH	Temp	-5°F
Wind Direction	From the South	Line Pressure	25 psig
Worse Firing Case Scenario Stages 1 – 6 firing 59 small tips Stages 7 – 11 firing 185 medium tips 8 ft 6 inches tip elevation		Flow Rate	1,096,600 lb/hr
		Composition	Volume %
		Ethylene	94%
		Ethane	6%

Case C2 (Base Case 2) Model Input

Parameter	Value	Flare Gas	Value
Ambient Temperature	95°F	MW	28.2
Ambient Pressure	14.7 psia	L.H.V.	1,508 BTU/SCF
Wind Speed	10 MPH	Temp	-5°F
Wind Direction	From the South	Line Pressure	25 psig
Stages 1-6 firing 120 small tips Stages 7-11 firing 185 medium tips 8 ft 6 inches tip elevation Assess Startup firing with one runner firing		Flow Rate	216,147 lb/hr
		Composition	Volume %
		Ethylene	94%
		Ethane	6%

Case C3 (Base Case 3) Model Input

Parameter	Value	Flare Gas	Value
Ambient Temperature	95°F	MW	19.4
Ambient Pressure	14.7 psia	L.H.V.	1,404 BTU/SCF
Wind Speed	10 MPH	Temp	-5°F
Wind Direction	From the South	Line Pressure	23.8 psig
Stages 1-8 firing 120 small tips 8 ft 6 inches tip elevation Assess startup firing with two runners firing low ethylene flare gas		Flow Rate	287,000 lb/hr
		Composition	Volume %
		Hydrogen	33.1%
		Ethane	23.1%
		Ethylene	36.5%
		Methane	5.7%
		Propylene	0.60%

 doi:10.20944/preprints202606.0243.v1

Simulation results from each case were evaluated with results used to develop recommended design and operating guidelines for MPGFs, which are now discussed. To ensure comparable results, the same methodology was followed for each case.

First, since all simulations were transient, to ensure the flare was operating with a steady wind profile blowing over the flare field, each simulation was run for approximately 10 to 15 seconds of flare operating time (approximately 3-4 days CPU time) before introducing flare gas to the flare burners. Once a steady wind profile was established and flare gas was burning at a steady rate, the simulations were run for another 15-20 seconds additional operating time (2-3 additional days CPU time). This "burn-time" (approximately 25 – 35 seconds) allowed the predicted flames above the flare burners caused by interaction between the wind and the flare structure to reach a quasi-steady condition. Following this procedure, each case conducted took approximately 5 - 7 CPU days to run before the results were ready to post-process to prepare the images shown.

Since a transient solver is used in *C3d*, all field variables fluctuate in time due to turbulence and other non-linear effects caused by coupling of the partial differential equations describing conservation of mass, momentum, and energy in the MPGF. Using the procedure described above, once the flare reached the "burning time" no continuously increasing (decreasing) trends were observed in any of the predicted variables. Instead, random fluctuations associated with turbulent fluctuations in the flow field were observed. This further confirmed "quasi-steady state" operation.

The convergence criteria chosen for all simulations was based on the equation of state always satisfied to within 0.01% or less at any location in the computational domain. Typically, this convergence criterion was better than the maximum allowable since the time step constraint was limited by the Courant condition, which allows the flow field to be solved to a higher degree of accuracy.

Base Cases Results

Several CFD cases (see Table 3) were used to assess the initial MPGF design and compare predicted performance for various base load firing conditions. This work was performed to examine the factors leading to observed damage to an operating MPGF (see Figure 16). The damaged runners that feed flare gas to the flare burners appear to have been damaged by excessively high surface temperatures, well above the design limit, which likely resulted in the catastrophic failure shown. Review of the MPGF operation log indicated this MPGF operated for a few weeks with flaring-rate gradually increasing from the normal startup firing rate (approximately 217,000 lb/hr) to about 25% of the emergency design flow (approximately 287,000 lb/hr). At the higher flow rate, the ethylene concentration in the flare gas decreased. The observed flare flames produced my the operating MPGF for these operating conditions were reported to be very long and dark indicating high soot levels in the flames. It is well known that high soot levels generate excess radiation flux from the flame which would create higher surface temperatures on the flare gas runners. These high temperatures would eventually cause excessive coking inside the runners, burner risers, and burners tips that would eventually lead to excessive damage of the MPGF as documented in Figure 16.

 doi:10.20944/preprints202606.0243.v1

Figure 16. Heat damage to MPGF runners (courtesy Zeeco, Inc.).

When an MPGF fires unsaturated flare gas, excessive soot is produced with high radiation flux to surrounding surfaces. One performance metric used to quantify flame radiation discussed earlier was intended to quantify the impact soot concentration has on flame radiation and its impact on the fence and ground surface temperatures. Test results from the validation study showed that about 12% radiation loss from a flare flame is common under non-sooting operation. Higher flame soot concentration caused by firing flare gas with unsaturated hydrocarbons (i.e., ethylene) were observed to have higher radiation loss from the flame. Higher flame radiation loss associated was also associated with lower combustion efficiency.

The initial base case conducted in this study considered a firing rate of 1,096,600 lb./hr. of flare gas with 94mol% ethylene (Table 4). All base cases examined in this work included a 10mph crosswind blowing from the south.

Observed damage to the flare gas runners was likely caused by continuous firing during start-up operation of the flare. A second and third base case considered different numbers of flare burners and different burner sizes with different row configurations. Tips with both smaller and larger flow areas were used in the base case simulations. The third base case (Case C3) included burners on two operating runners firing flare gas with an slightly higher firing rate of high hydrogen (33.1%) flare gas.

CFD input for all three of these base cases are provided in Table 4. Results show predicted flame shape and size (see Figure 17) plus predicted surface and fence temperatures (see Figure 18). These results demonstrate the impact each design feature has on operation of this MPGF.

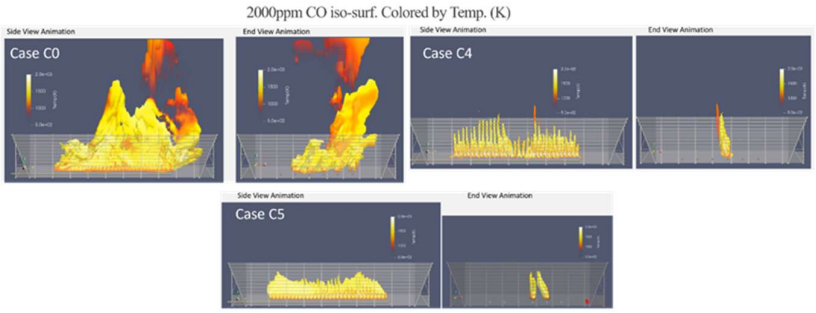

Figure 17. Predicted flame shape and height for base cases (side and end views).

 doi:10.20944/preprints202606.0243.v1

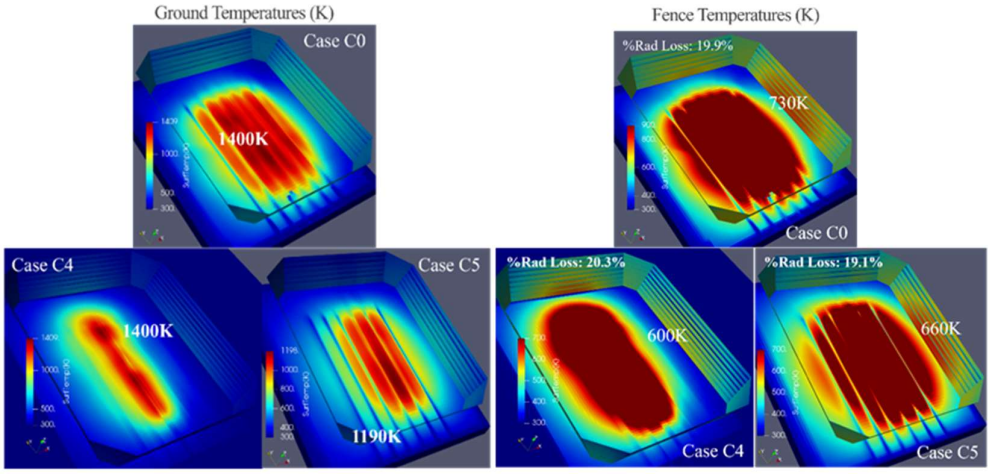

Figure 18. Predicted ground and Fence temperature for base cases (perspective view).

Comparing graphical (Figure 17 and Figure 18) and numerical results (Table 5) for these base cases, the main effect on flare operation appears to be related to flare gas flowrate and ethylene concentration. High flow and high ethylene concentration resulted in the highest radiation flux from the flame to surrounding surfaces as shown by the highest predicted fence temperature. As expected, the higher flare gas firing rate produced the tallest flames leading to the highest predicted ground temperature (1400K) and fence temperature (730K). The predicted ground temperature for this flame was also the highest. Given this case had ethylene rich flare gas, more soot was produced in the flame than the other two cases which implies the flow and ethylene concentration was likely the root cause for damage to the flare gas runners shown in Figure 16. A counter intuitive result was that the fence temperature for the low flow/low ethylene fuel case (Base Case 3) was 660K compared to 600K for the low flow/rich ethylene base case (Base Case 2) while the fence temperature for Base Case 1 was 770K. Also, the predicted ground temperature for Base Case 3 was 1190K while the ground temperature for Base Case 2 was 1400K. Considering the predicted flame size was approximately the same for both Base Case 2 and Base Case 3 implies that although flame size has a significant effect on fence and surrounding surface temperatures, ethylene concentration has the greatest impact on ground temperature. Also, since DRE is directly related to flame temperature, ethylene rich flames are likely to produce more emissions and have lower combustion efficiency. This conclusion is consistent when one compares the %radiation loss from the flame (20.3% for Base Case 2 compared to 19.1% for Base Case 3). Since flame radiation loss is directly related to flame soot concentration, the high soot levels in Base Case 2 means more flame radiation loss compared to Base Case 3, due to lower soot concentration in Base Case 2 and that Base Case 3 has lower Combustion Efficiency.

Table 5. Predicted MPGF Performance for Base Cases 1 -3.

Case #	Radiation loss from flame (%)	Fence Temperature (K)	Ground Temperature (K)	Firing Rate (lb/hr)
C1 (Base Case 1)	19.9	730	1400	1,096,600
C2 (Base Case 2)	20.3	600	1400	216,147
C3 (Base Case 3)	19.1	660	1190	287,000

Given the simulation's ability to reproduce the observed conditions that would lead to excessive surface temperature and associated system damage, the code was used to analyze various design options to remedy this issue.

 doi:10.20944/preprints202606.0243.v1

Design Case Results

Given the base case results, the overall MPGF design was evaluated considering different design options and operating conditions (see Table 6). The approximate MPGF design configuration for each design case is shown in terms of number and size of flare burners, fuel staging arrangement by row, and use of assist-media (see Figure 19 for D1-D2, Figure 20 for D3, Figure 21 for D4, Figure 22 for D5, Figure 23 for D6). These cases examined tip size, row spacing, lower wind fence porosity, and the impact of using steam assist in the flare burners. Model input for each of these design cases are provided in Table 7. Results from these cases were used to quantify the impact of these design features. All flare burner tips were located at an elevation of 8.5 ft (2.6 m) above ground level of the flare field. The predicted flame shape and size for each case are shown in Figure 24. The predicted ground and fence temperatures are shown in Figure 25. The objective of the design analysis was to assess the impact of key design features on MPGF performance with the goal of reducing flare damage and improving combustion efficiency.

Table 6. Description of MPGF design cases.

Case Name (running case #)	Description
D1 (4)	Full firing rate with high ethylene flare gas, 368 tips with extended runners and small stages relocated near fence (288 small tips + 80 medium tips)
D2 (5)	Full firing rate with high ethylene flare gas, 398 small tips on extended runners.
D3 (6)	Full firing rate with high ethylene flare gas, redistributed tip layout of 298 medium sized tips.
D4 (7)	Full firing rate of high ethylene flare gas, 153 large tips with first/last row moved 2 ft outward toward wind fence.
D5 (8)	Full firing rate of high ethylene flare gas, 298 medium tips with 450 lb/hr of 50 psig steam assist added to start up runners (stages 1-9).
D6 (9)	Full firing rate of high ethylene flare gas, 398 small sized tips with modified lower wind fence up to 18 ft elevation.

Table 7. CFD input for Design Cases D1 – D6.

Design Cases D1 – D6: Model Conditions

Parameter	Value	Composition	Volume %	Flare Gas	Value
Ambient Temperature	95°F	Ethane	6%	MW	28.2
Ambient Pressure	14.7 psia	Ethylene	94%	L.H.V.	1,508 BTU/SCF
Wind Speed	10 MPH			Temp	-5°F
Wind Direction	From the South			Avail. Pressure	25 psig
				Flow Rate	1,096,600 lb/hr

D1: 288 small sized tips and 80 medium sized tips
D2: 398 small sized tips
D3: 298 medium sized tips
D4: 153 large sized tips
D5: 298 medium tips w/ steam assist added to startup runners (Stages 1-9)
D8: 398 small sized tips

 doi:10.20944/preprints202606.0243.v1

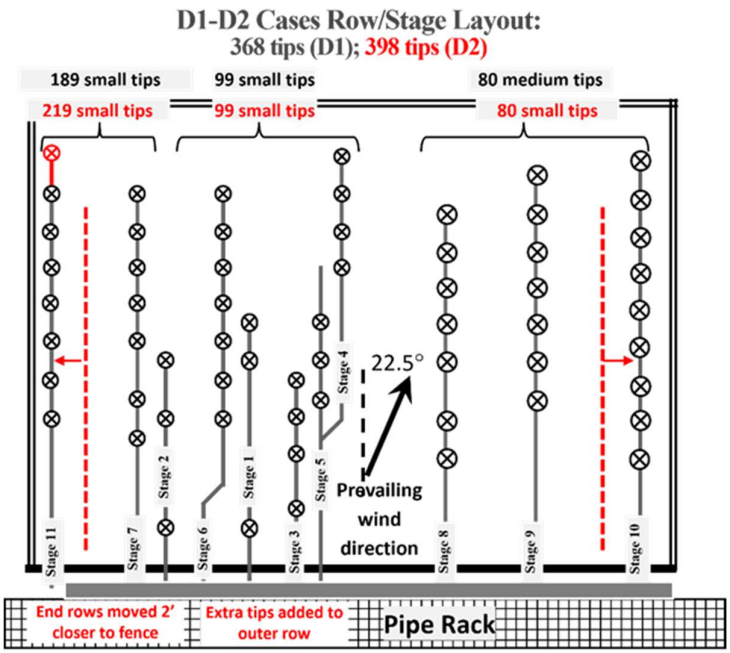

Figure 19. MPGF design configuration 1 (row spacing increase with small & medium tips) and 2 (row spacing increase with all small tips).

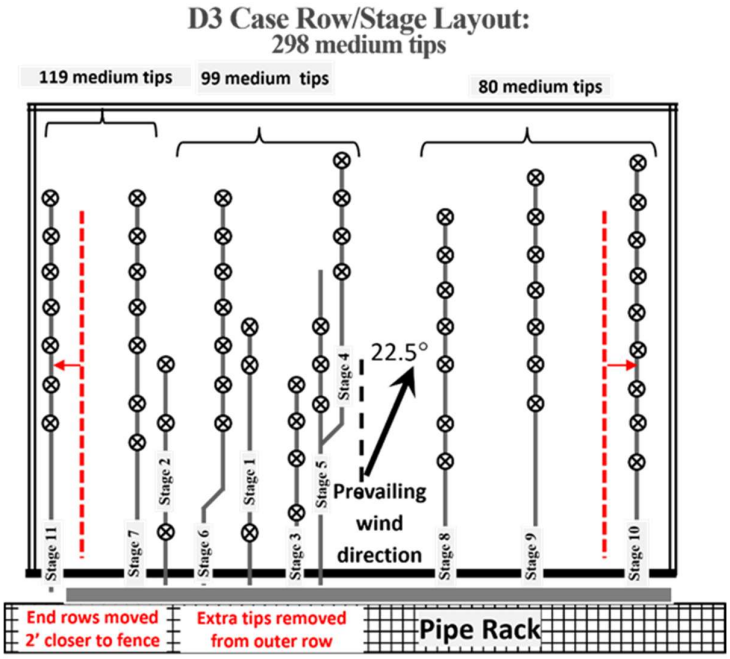

Figure 20. MPGF design configuration 3 (row spacing increased and all medium tips).

 doi:10.20944/preprints202606.0243.v1

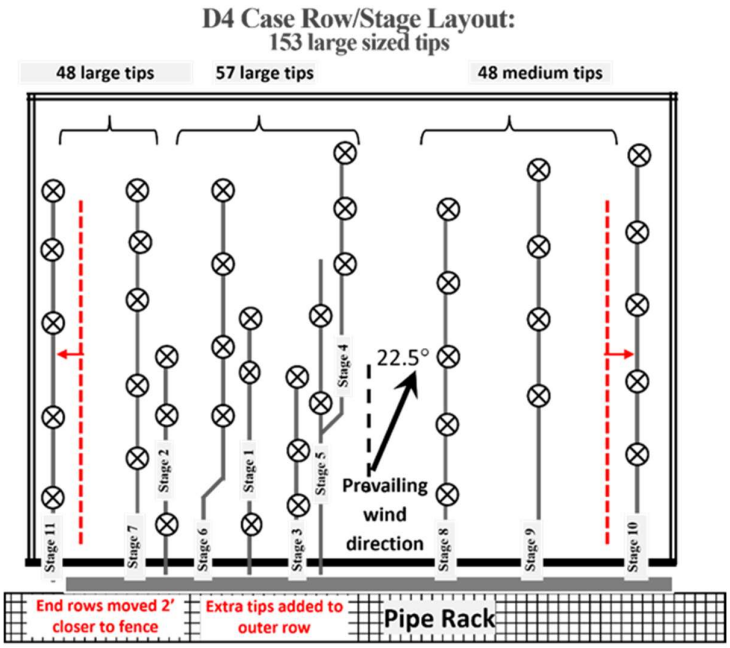

Figure 21. MPGF design configuration 4 (fewer larger burners).

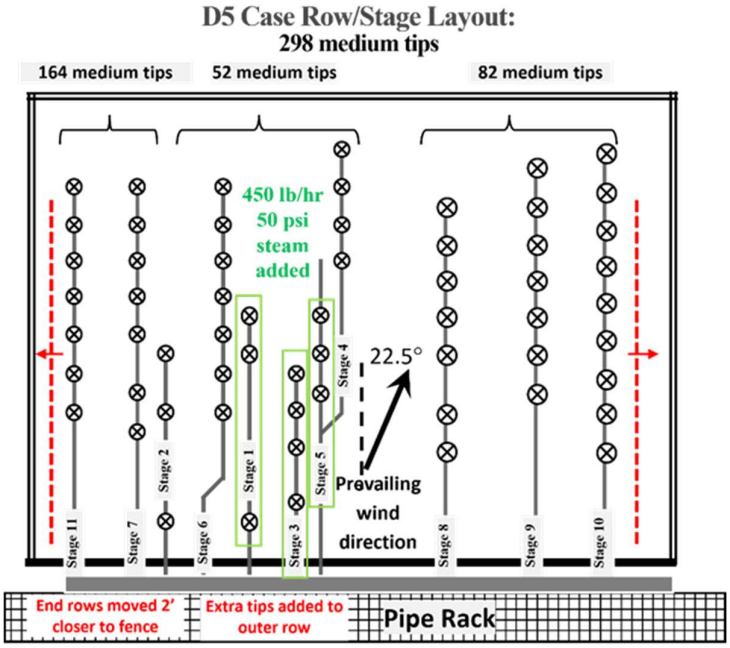

Figure 22. MPGF design configuration 5 (steam assist included).

 doi:10.20944/preprints202606.0243.v1

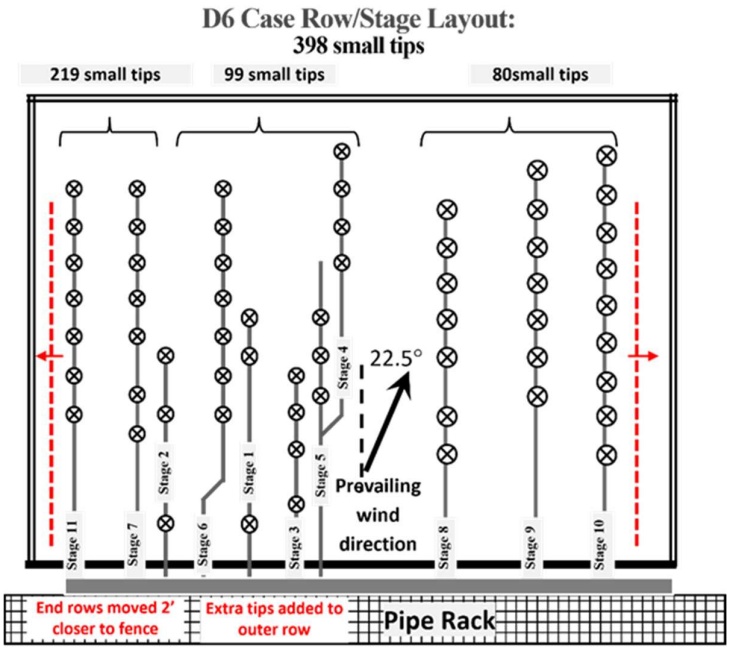

Figure 23. MPGF design configuration 6 (lower wind fence modification).

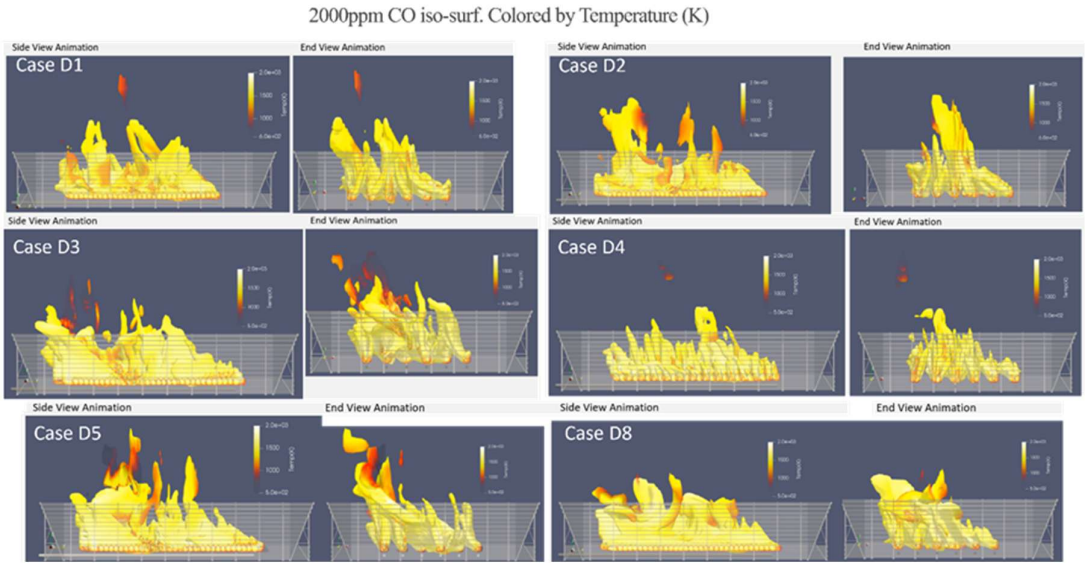

Figure 24. Predicted flame shape and height for design cases (side and end views).

 doi:10.20944/preprints202606.0243.v1

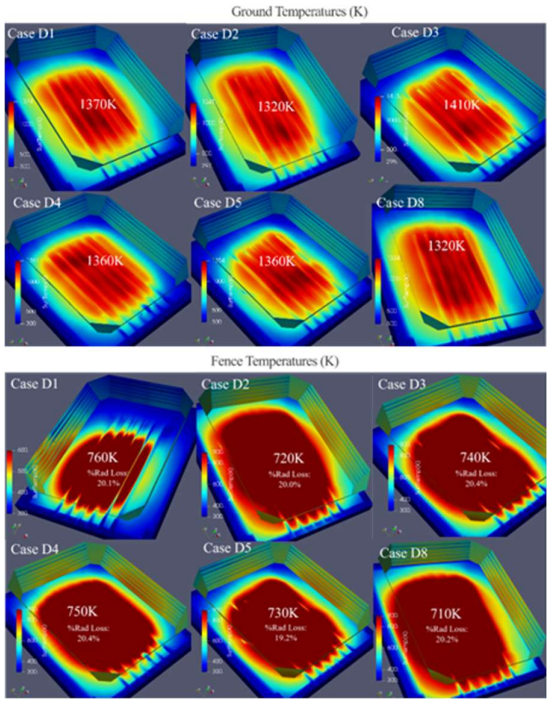

Figure 25. Predicted ground and Fence temperature for design cases (perspective view).

Whereas the original MPGF design used 366 tips (57 small tips and 309 large tips), the Design cases considered using more small burner tips in a spare stage, with an extended runner also using small tips. Rows in this smaller stage were moved closer to the wind fence adding extra space between adjacent burner rows. Results from each design case were analyzed to assess the impact of tip size, tip and row spacing, distance of burner rows to the fence, flare gas firing rate, and flare gas composition on MPGF operation (Table 8). Results from these Design cases are now discussed.

Table 8. Predicted MPGF Performance in Design Cases.

Case #	Radiation loss from flame (%)	Fence Temperature (K)	Ground Temperature (K)	Firing Rate (lb/hr)
D1	20.1	760	1370	1,096,600
D2	20.0	720	1340	1,096,600
D3	20.4	740	1410	1,096,600
D4	20.4	750	1360	1,096,600
D5	19.2	730	1360	1,096,600
D6	20.2	710	1320	1,096,600

Whereas the original MPGF design used 366 tips (57 small tips and 309 large tips), the Design cases considered using more small burner tips in a spare stage, with an extended runner also using small tips. Rows in this smaller stage were moved closer to the wind fence adding extra space between adjacent burner rows. Results from each design case were analyzed to assess the impact of tip size, tip and row spacing, distance of burner rows to the fence, flare gas firing rate, and flare gas composition on MPGF operation (Table 8). Results from these Design cases are now discussed.

The first two design cases (D1 and D2) represented an MPGF design using all small flare burner tips compared to a design using a mix of small and medium tips on longer runners located closer to the wind fence. These cases evaluated how tip size and runner spacing would impact fence and ground temperature, flame shape and size, and %radiation lost from the flame. The third design case

 doi:10.20944/preprints202606.0243.v1

(D3) used all medium sized tips redistributed on the existing runners used in the original MPGF design. This case evaluated the impact of tip size without changing runner length. The fourth design case (D4) used only large tips arranged on the existing runners with a spare runner added and the first and last rows moved 2 ft (0.61 m) closer toward the adjacent fence. This case further assessed the impact of tip size and row location on MPGF performance. The fifth design case (D5) used all medium tips with steam-assist added to the startup stages to improve air entrainment and combustion efficiency by reducing soot formation. This case evaluated the impact assist media has on MPGF performance. The last design case (D6) used all small tips arranged on available runners in the original MPGF design. Results of each of these design cases are discussed below to identify those design changes with the biggest impact on flare performance.

Case D5 included steam assist in the start-up runners to enhance combustion efficiency. Steam injection is known to enhance air entrainment into the flame which reduces soot formation and associated flame radiation. This behavior is observed when all flare burner tips are firing in a large multi-point ground flare. Reducing radiation from the flame also reduces surface temperature on the wind fence, flare runners, and nearby equipment. This reduces high-temperature damage and extends the useful life of an MPGF. Steam assist reduces soot formation that results in less flame radiation. This should mean that the ground temperature would decrease as well but it is not predicted to do so. Steam assist also adds upward momentum to a burner flame that would decrease flame deflection and reduce interaction with nearby flames. For Case D5, burner flames in Stages 1-9 with steam assist have more upward momentum so these flames are not deflected as much as flames without steam assist. Less flame deflection should result in less radiation to the ground and lower ground temperature. The steam assist effect was further investigated using two subsequent cases in the final analysis phase of this work.

Optimization Case Results

After evaluating the impact of various MPGF design features, the overall MPGF design was optimized using *C3d*. This phase included performing eleven additional CFD simulations (see Table 9) to find the optimal design of an MPGF in terms of combustion efficiency, flare operating life, and process safety. Design options considered in these cases included:

1. Flare burner port area and its impact on number or tips and tip spacing / sqrt (port area),
2. Spacing between adjacent burner rows and its impact on start-up operations,
3. Burner tip elevation above ground level and its impact on fence and ground temperature, and
4. Wind fence porosity and its impact on flame size, shape and soot production.

Table 9. Description of the optimization cases.

Case Name (running case #)	Case Description Flare Tip size: "4"=medium sized tip; "5"=small sized tip Firing rate: "a" = 300,000 lb/hr high H2 concentration; "f" = 1,096,600 lb/hr high C2H4 concentration Assist media: "aa" = air assist media used; "sa" = steam assist media used Fence modifications: "f1" = modified lower fence; "f2" = modified lower fence and upper stadium fence
E4a-na-f1-e1 (10)	56 large tips, H2 rich gas, startup firing rate, standard tip elevation, increased runner spacing, lower fence modified, no assist media
E5a-na-f1-e1 (11)	72 small tips, H2 rich gas, startup rate, standard tip elevation, standard runner spacing, lower fence modified, no-assist media
E4f-na-f1-e1 (12)	184 medium tips, ethylene rich gas, emergency firing rate, 4 extra rows, standard tip elevation, increased runner spacing, lower fence modified, no-assist media
E4f-na-f2-e1 (13)	184 medium tips, ethylene rich gas, emergency firing rate, 4 extra rows, standard tip elevation, increased runner spacing, full fence modified, no-assist media
E4f-sa-f2-e2 (14)	184 medium tips, ethylene rich gas, emergency firing rate, 4 extra rows, higher tip elevation, increased runner spacing, full fence modified, steam-assist media
E4f-aa-f2-e2 (15)	184 medium tips, ethylene rich gas, emergency firing rate, 4 extra rows, higher tip elevation, increased runner spacing, full fence modified, air-assist media
E5f-na-f1-e1 (16)	252 small tips, ethylene rich gas, emergency firing rate, 4 extra rows, standard tip elevation, increased runner spacing, lower fence modified, no-assist media
E5f-na-f2-e1 (17)	252 small tips, ethylene rich gas, emergency firing rate, 4 extra rows, standard tip elevation, increased runner spacing, full fence modified, no-assist media
E5f-na-f2-e2 (18)	252 small tips, ethylene rich gas, emergency firing rate, 4 extra rows, higher tip elevation, increased runner spacing, full fence modified, no-assist media
Ef5-sa-f2-e2 (19)	252 small tips, ethylene rich gas, emergency firing rate, 4 extra rows, higher tip elevation, increased runner spacing, full fence modified, steam-assist media
E5f-aa-f2-e2 (20)	252 small tips, ethylene rich gas, emergency firing rate, 4 extra rows, higher tip elevation, increased runner spacing, full fence modified, air-assist media

Results from these optimization cases illustrate the impact of each of several design options. Cases listed in Table 10 are named based on the different design options included in the MPGF

 doi:10.20944/preprints202606.0243.v1

design. For example, the size of the flare tip used is indicated by "**4**" for large tips verses "**5**" for smaller tips. The relative tip elevation used is indicated by "**e1**" for standard tip elevation and "**e2**" for higher tip elevation. Wind fence design is specified by "**f1**" for a modified lower wind fence with higher porosity while "**f2**" refers to a fence with both the lower portion and the upper portion modified. Several cases were conducted using either air or steam assist-media to improve combustion efficiency. This was indicated by "**aa**" for air-assist and "**sa**" for steam-assist media ("**na**" was used to indicate no assist media was used)[2].

Table 10. CFD input for Optimization E4a and E5a Cases.

Optimization E4a and E5a Cases: Model Conditions

Parameter	Value	Composition	Volume %	Flare Gas	Value
Ambient Temperature	95°F	Ethane	6%	MW	28.2
Ambient Pressure	14.7 psia	Ethylene	94%	L.H.V.	1,508 BTU/SCF
Wind Speed	10 MPH			Temp	-5°F
Wind Direction	From the South			Avail. Pressure	25 psig
				Flow Rate	300,000 lb/hr

E4a-na-f1-e1: 56 large tips, standard tip elevation, increased runner spacing, lower fence modified, no assist media

E5a-na-f1-e1: 72 small tips, standard tip elevation, standard runner spacing, lower fence modified, no-assist media

Naming Legend:
Flare Tip size: "4"=medium sized tip; "5"=small sized tip
Firing rate: "a" = 300,000 lb/hr high H2 concentration; "f" = 1,096,600 lb/hr high C2H4 concentration
Assist media: "aa" = air assist media used; "sa" = steam assist media used
Fence modifications: "f1" = modified lower fence; "f2" = modified lower fence and upper stadium fence

Case 10 (E4a-na-f1-e1) and Case 11 (E5a-na-f1-e1) examined the effect of tip size and runner spacing for startup firing conditions (lower flare gas flow rate). Case 12 (E4f-na-f1-e1) through Case 20 (E5f-aa-f2-e2) examined the effect of assist media, row spacing, tip size, tip elevation, and wind fence design under emergency firing conditions. Results from all eleven optimization cases were analyzed and results are summarized below and form the basis for the recommended "optimum" MPGF design.

The flame shape and size for Case E4a and Case E5a along with predicted ground surface temperature and inner wind fence temperature are shown in Figure 26 and Figure 27.

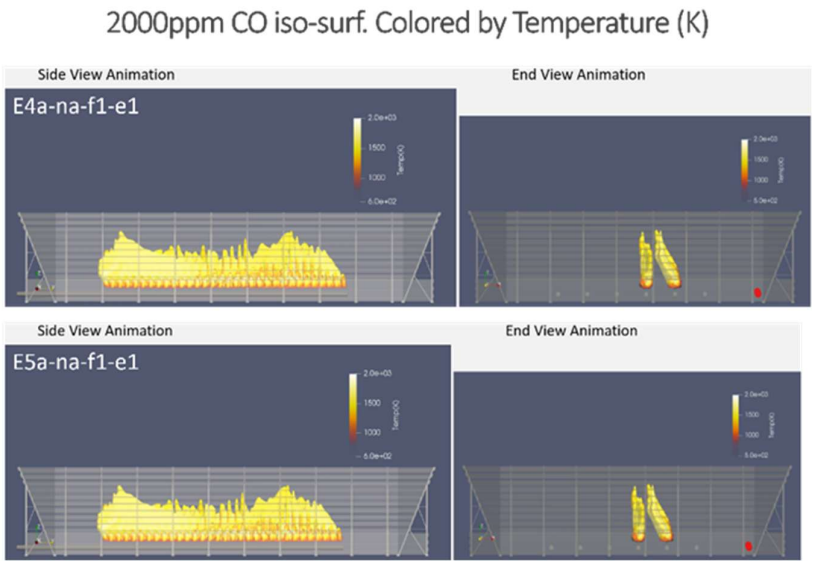

Figure 26. Predicted flame shape and size for cases E4a and E5a (tip size effect).

[2] Note: assist media was only included in the startup runners.

 doi:10.20944/preprints202606.0243.v1

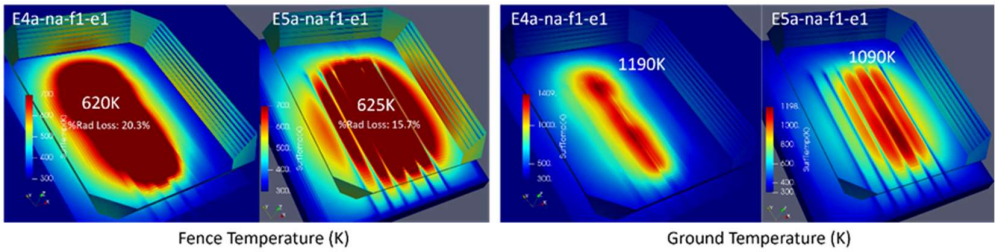

Figure 27. Predicted surface temperatures for cases E4a and E5a (tip size effect).

Examining the key metrics for these cases (see Table 11), it appears tip size does not impact predicted flame size and shape. The predicted wind fence temperature is only slightly higher for smaller tips than large tips (625K vs 620K). Radiation loss from flame is significantly lower for small tips compared to large tips (15.7% vs 20.3%). Predicted ground temperature is significantly lower for small tips compared to large tips (1090K vs 1190K), consistent with less radiation loss from the flame. Given that these two cases were for startup firing rate, significantly lower than the emergency firing rate, tip size is expected to have much less effect on flame shape and size as predicted. In summary, for startup firing conditions, tips size mainly affects flame radiation loss which mainly affects ground temperature but does not significantly impact flame shape and associated fence temperature.

Table 11. Predicted MPGF Performance for Optimization E4a and E5a Cases.

Summary: Radiation and Temperature Results
E4a and E5a Cases

Case #	Radiation loss from flame (%)	Fence Temperature (K)	Ground Temperature (K)	Firing Rate (lb/hr)
E4a	20.3	620	1190	300,000
E5a	15.7	625	1090	300,000

Predicted flame shape and size for Case E4f-na-**f1**-e1 (lower fence modified only) and Case E4f-na-**f2**-e1 (both lower and upper fence modified) both use larger tips and show little impact from wind fence design (see Figure 28 and Figure 29). Predicted metrics shown in Table 12 confirm these observations. For different wind fence designs, flame radiation loss varies from 19.2% to 21.2% while predicted fence temperature changes from 840K to 770K and predicted ground temperature changes from 1355K to 1330K. Based on this, it is concluded that no additional benefit is achieved by modifying the upper wind fence and changes to the lower fence are most important.

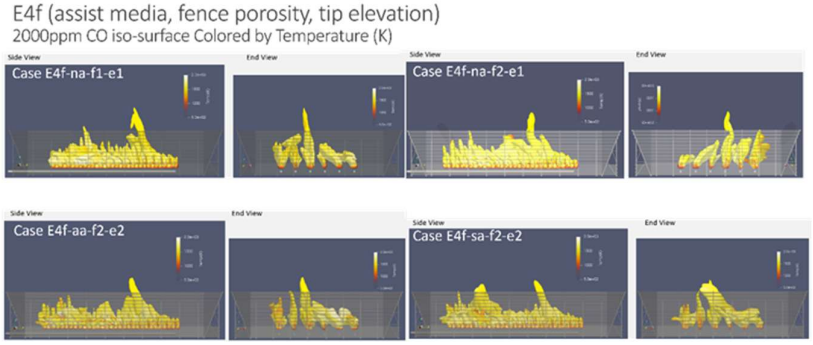

Figure 28. Flame size and shape for E4f cases.

 doi:10.20944/preprints202606.0243.v1

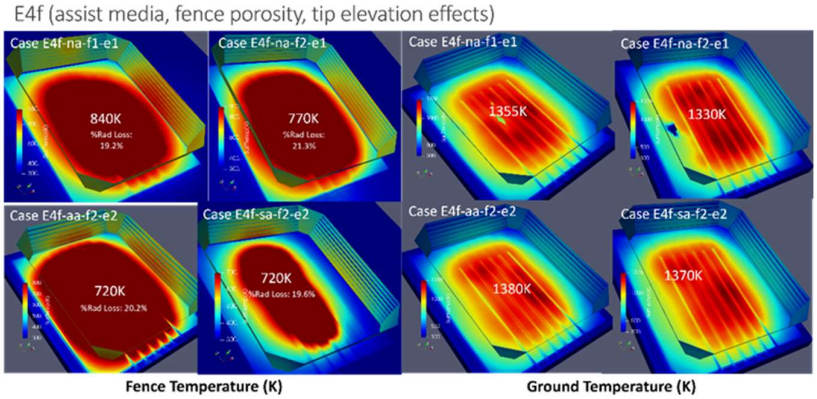

Figure 29. Fence and Ground Temperatures for Cases E4f.

Table 12. Predicted MPGF Performance for Optimization E4f and E5f Cases.

Summary: Radiation and Temperature Results
E4f and E5f Cases

Case #	Radiation loss from flame (%)	Fence Temperature (K)	Ground Temperature (K)	Firing Rate (lb/hr)
E4f-na-f1-e1	19.2	840	1355	1,096,600
E4f-na-f2-e1	21.2	770	1330	1,096,600
E4f-sa-f2-e2	19.6	720	1370	1,096,600
E4f-aa-f2-e2	20.2	720	1380	1,096,600
E5f-na-f1-e1	20.4	740	1340	1,096,600
E5f-na-f2-e1	19.3	730	1320	1,096,600
E5f-na-f2-e2	18.8	720	1320	1,096,600
E5f-sa-f2-e2	18.8	710	1310	1,096,600
E5f-aa-f2-e2	17.6	710	1340	1,096,600

Flame shape and size show little difference when using air-assist (Case E4f-**aa**-f2-e2) versus steam-assist (Case E4f-**sa**-f2-e2) when using larger tips. Predicted flame radiation loss for air-assist is 20.2% versus 19.6% for steam-assist while fence temperature is 720K for both and ground temperature is 1380K for air-assist and 1370K for steam-assist. Based on these observations, the conclusion is that steam or air-assist have the same basic effect of increasing air entrainment into the flame which improves combustion efficiency and reduces smoke formation.

For cases using smaller tips (E5f cases), the impact of modifying the upper wind fence had little impact on MPGF performance (see Figure 30 and Figure 31). Case E5f-na-**f1**-e1 (lower fence modification) versus Case E5f-na-**f2**-e1 (lower and upper fence modification) shows flame radiation loss of 20.4% versus 19.3%, fence temperature of 740K versus 730K, and ground temperature of 1340K versus 1320K (see Figure 32 and Figure 33). Considering the same conclusion was drawn for cases using larger tips, the overall conclusion is that modifying the lower fence is sufficient.

 doi:10.20944/preprints202606.0243.v1

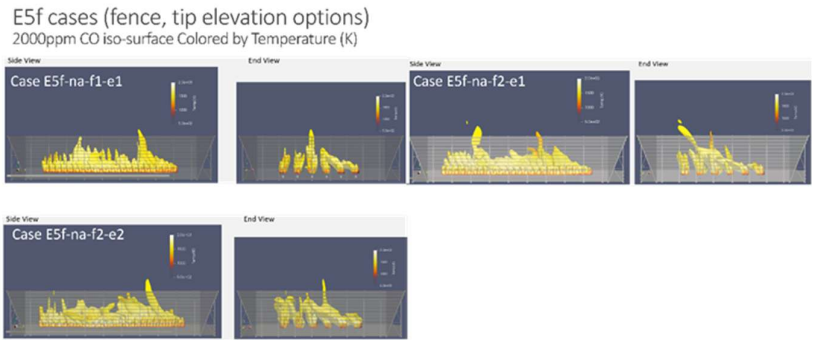

Figure 30. Flame size and shape for E5f cases without assist-media.

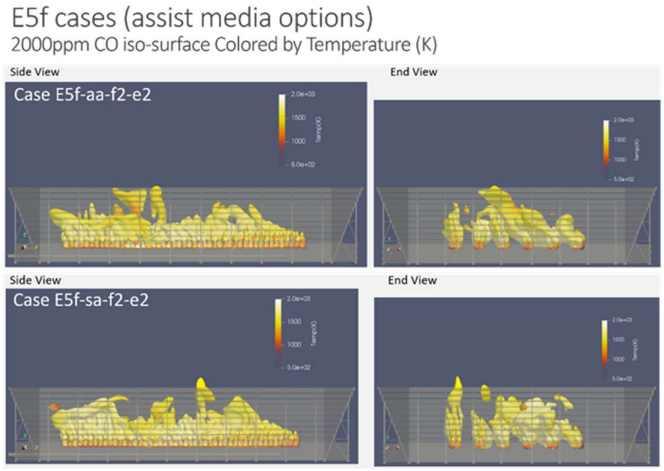

Figure 31. Flame shape and size for E5f case with assist-media.

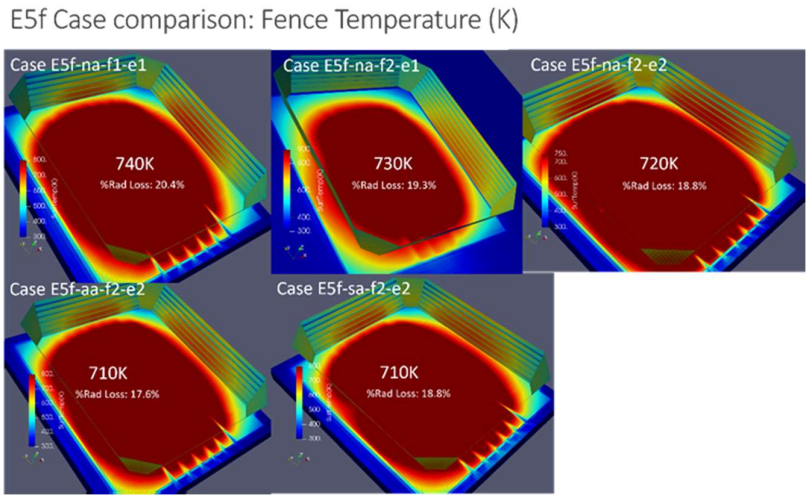

Figure 32. Fence temperatures for cases E5f.

 doi:10.20944/preprints202606.0243.v1

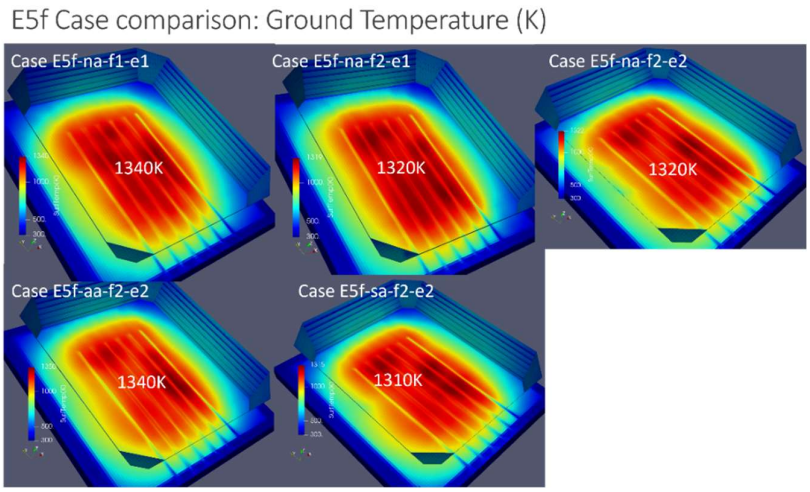

Figure 33. Ground temperatures for cases E5f.

Flame shape and size for cases where the tip elevation was higher above ground level (Case E5f-na-f2-**e1** versus Case E5f-na-f2-**e2**) showed no noticeable effect. Predicted metrics for both cases confirmed this observation with flame radiation loss of 19.3% versus 18.8%, fence temperature of 730K versus 720K, and both ground temperatures of 1320K. Thus, tip elevation above ground level was concluded to have little effect as well.

The flame size and shape for MPGF using smaller tips with assist-media were very similar. Predicted metrics for Case E5f-**sa**-f2-e2 and Case E5f-**aa**-f2-e2) were flame radiation loss of 18.8% versus 17.6%, predicted fence temperature were both 710K, and ground temperature of 1310K versus 1340K. Since this was the same conclusion for cases with larger tips, the overall conclusion is that the type of assist-media is not important.

Summary and Conclusions

Multi-Point Ground Flares represent a special class of flares used to safely and efficiently process large volumes of flammable gas produced in petroleum processing facilities. This paper presented a brief history of the development of the MPGF and highlights of specific design features including:

1. The ability to fire high rates of flare gas over longer periods of time cleanly and safely,
2. Staged operation that facilitates a large turn-down range so they can process very high flow rates of varied flare gas composition with an wide range of tip pressures and gas temperatures,
3. Relative distance between the MPGF field and nearby process equipment and personnel that ensure safe operation for high radiation flux from the flame during high firing rates,
4. Engineered wind fence designs that efficiently protect equipment and personnel from flame radiation during high firing rates,
5. Efficient wind fence design to allow sufficient air entrainment into the flame to promote clean efficient combustion for standard and non-standard flare gas composition, variable operating pressures and temperature, under high ambient wind conditions,
6. Reduced noise emissions from operating flares to lessen their impact on workers and the surrounding community, and
7. Engineered flare burner tips that promote local air/fuel mixing to support clean, efficient combustion.

This paper also presented results of an extensive CFD analysis of an operating MPGF located in Port Arthur, Texas (USA) which included hundreds of flare burner tips arranged in a large flare field. The MPGF analysis included normal wind conditions for startup and emergency firing conditions for flare gas with high percentages of hydrogen and ethylene. Details of this analysis including a brief

 doi:10.20944/preprints202606.0243.v1

description of the CFD tool used in this study along with the methodology used to quantify MPGF performance were presented. Previous validation results for the flare simulation tool were also presented. Simulation results from this work have led to the following recommended design and operation guidelines including:

1. Flame height, shape, and smokeless performance are greatly affected by tip spacing and row spacing,
2. Higher fence porosity reduces flame height and soot formation because flames are better aerated,
3. MPGFs equipped with air- and steam-assisted flare tips operate more efficiently compared to normal MPGFs using standard pressure assisted flare tips,
4. Tip port area and tip spacing dramatically effect predicted radiation flux to the ground but less significantly impact radiation flux to the fence,
5. Tip size impacts DRE at full firing rate but less so at lower rates during startup, and
6. Radiation flux without direct-line-of-sight to outside the wind fence is minimal.

Specific system details that were included in this analysis included:

- The MPGF was constructed on an elevated berm giving it approximately 17’ elevation above surrounding grade,
- The wind fence was modified by removing three panels from lower personal safety fence with the upper stadium wind fence further modified by removing additional panels to increase fence porosity,
- The standard tip elevation of 8’6” was raised to 10’6”,
- Tip flow areas considered included 1.33 (small size), 2.7 (medium size) and 3.48 sq-in (large size),
- Steam assist and air assist media was included in the startup tips, and
- Full emergency firing rate was 1,096,600 lb/hr flare gas flow with 94 mol% ethylene composition. Startup firing rates considered included 180,000 lb/hr and 300,000 lb/hr with startup composition.

In summary, well designed and operated MPGFs are capable of processing large quantities of flammable hydrocarbon flare gas safely and efficiently. The recommendations provided in this paper can be used to help design and operate MPGF to ensure they don’t “burn down” their flare system.

Author Contributions: Conceptualization, J. Smith, J. Dugué and F. Euzenat; Writing-Review & Editing, J. Smith and J. Dugué; Methodology, V. Sreedharan, J. Smith, A. Suo-Antilla and Z. Smith; Software, A. Suo-Antilla; Validation, A. Suo-Antilla, J. Smith and Z. Smith; Writing-Original Draft Preparation, J. Smith, J. Dugué and Z. Smith; Visualization, V. Sreedharan, J. Smith, A. Suo-Antilla and Z. Smith; Supervision, J. Smith.

Findings: This work was based on several years of work by Elevated Analytics supported by Zeeco Corporation with external funding provided by TotalEnergies.

Acknowledgments: We wish to acknowledge editorial support provided by Mrs. Eileen Smith in revising and giving editorial advice for manuscript revision. The authors also acknowledge editorial comments provided by engineers at Zeeco Corporation and TotalEnergies.

References

[1] J. Smith, Jackson, R.E., Z. Smith, D. Allen and S. Smith, "Transient Ignition of Multi-Tip Ground Flares," in *AFRC Combustion Symposium*, University of Utah, Salt Lake City, Utah, September 17- 19 (2018).

 doi:10.20944/preprints202606.0243.v1

[2] J. D. Smith, R. Jackson, A. Suo-Antilla, S. Smith and D. Allen, "Achieving Environmental Compliance through Proper Destruction Efficiency of Low-Profile Multi-Tip Flare Systems," in *American Flame Research Committees-Industrial Combustion Symposium*, Hyatt Regency Hotel Houston, Texas, September 2014.

[3] J. Smith, A. Suo-Antilla, N. Philpott and S. Smith, "Prediction and Measurement of Multi-Tip Flare Ignition," in *American Flame Research Committees - International Pacific Rim Combustion Symposium, Advances in Combustion Technology: Improving the Environment and Energy Efficiency*, Sheraton Maui, Hawaii, September 26 –29 (2010).

[4] J. Smith and H. J. R. Al-Hameedi, " Testing and Prediction of Flare Emissions Created during Transient Flare Ignition," *Int J Petrochem Res*, vol. 2, no. 2, pp. 175-181, 2018.

[5] J. Smith, J. Dugue, F. Euzenat, A. Suo-Antilla, Z. Smith and V. Sreedharan, "Analysis of Multi-Point Ground Flare Design and Operation: General Guidelines," in *Mathias Days 2022: Computational Science Engineering, Data Science & Artificial Intelligen*, Paris, France, October 3-6 (2022).

[6] M. Greiner and A. Suo-Anttila, "Validation of the ISIS Computer Code for Simulating Large Pool Fires Under a Varity of Wind Conditions,," *ASME J. Pressure Vessel Technology*, vol. 126, pp. 360-368, 2004.

[7] A. J. Suo-Anttila, "C3d Combustion Model Validation," Albuquerque, January 2019.

[8] J. Smith, A. Suo-Anttila, S. Smith and J. Modi, "Evaluation of the Air-Demand, Flame Height, and Radiation Load on the Wind Fence of a Low-Profile Flare Using ISIS-3D," in *AFRC-JFRC 2007 Joint International Combustion Symposium*, Marriott Waikoloa Beach Resort, Hawaii, October 21-24, 2007.

[9] J. Smith, R. Jackson, V. Sreedharan, A. Suo-Anttila, Z. Smith, D. Allen, D. DeShazer and S. Smith, "Safe Operation of Adjacent Multi-Point Ground Flares: Predicted and Measured Flame Radiation in Cross Flow Wind Conditions," in *AFRC Industrial Combustion Symposium*, Sheraton Kauai Resort, Kauai, Hawaii, September 9 –11, 2016.

 doi:10.20944/preprints202606.0243.v1

[10] J. Smith, Jackson, R.E., Z. Smith, D. Allen and S. Smith, "Transient Ignition of Multi-Tip Ground Flares," in *AFRC Industrial Combustion Symposium*, University of Utah, Salt Lake City, Utah, September 17- 19 (2018).

[11] D. J., R. B and H. T. , "Study of Quasi-Global Schemes for Hydrocarbon Combustion," *Combustion Science and Technology,* vol. 26, no. 1-2, pp. 1-15, 1981.

[12] K. I. K. and M. K., "A Numerical Study on Propagation of Premix Flames in Small Tubes," *Combustion and Flame,* vol. 146, pp. 283-301, 2006.

[13] J. Smith, R. Jackson, V. Sreedharan, A. Suo-Anttila, D. Allen and S. Smith, "Withstanding the Wind," *Hydrocarbon Engineering,* pp. 43-49, October 2016.

[14] J. Smith, B. Adams, R. Jackson and A. Suo-Anttila, "Use of RANS and LES Turbulence Models in CFD Predictions for Industrial Gas-fired Combustion Applications," *Journal of the International Flame Research Foundation,* December (2017).

[15] J. Smith, R. Jackson, A. Suo-Anttila, K. Hefley, Z. Smith, D. Wade, D. Allen and S. Smith, "Radiation Effects on Surrounding Structures from Multi-Point Ground Flares," in *AFRC Industrial Combustion Symposium*, Historic Fort Douglas Officers Club University of Utah, Salt Lake City, Utah, September 9-11, 2015.

[16] S. Fuss and A. Hamins, "An estimate of the correction applied to radiant flame measurements due to attenuation by atmospheric CO2 and H2O," *Fire Safety Journal,* vol. 37, pp. 181-190, 2002.

[17] J. Smith, R. Jackson, V. Sreedharan, Z. Smith and A. Suo-Antilla, "Lessons Learned from Transient Analysis of Combustion Equipment in the Process Industries," in *AFRC 2019 - Industrial Combustion Symposium*, Hilton Waikoloa Village, Hawaii, September 9-11, 2019.

[18] J. Smith, A. Suo-Anttila, V. Sreedharan and Z. Smith, "Simulation of the Thermal-Acoustic Coupling Inside an Industrial Hazardous Waste Incinerator," in *AFRC 2020 Industrial Combustion Symposium*, Houston, Texas (online), October 19-20, 2020.

 doi:10.20944/preprints202606.0243.v1

[19] C. Sondhauss, "About the Sound Vibrations of the Air in Heated Glass Tubes and in Covered Pipes of Unequal Width," *Ann Phy,* vol. 79, p. 1, 1850.

[20] J. Smith, A. Suo-Antilla, S. Smith and J. Modi, "Evaluation of the Air-Demand, Flame Height, and Radiation Load on the Wind Fence of a Low-Profile Flare Using ISIS-3D," in *AFRC-JFRC 2007 Joint International Combustion Symposium*, Marriott Waikoloa Beach Resort, Hawaii, 21 - 24 October, 2007.

[21] J. Smith, R. Jackson, A. Suo-Anttila, K. Hefley, D. Wade, D. Allen and S. Smith, "Prediction and Measurement of Multi-Tip Flare Ignition," in *" American Flame Research Committees 2013 – Industrial Combustion Symposium, Safe and Responsible Development in the 21st Century* , Sheraton Kauai, Hawaii, September 22 –25, 2013.

[22] D. Miller, "New Model for Predicting Thermal Radiation from Flares and High Pressure Jet Fires for Hydrogen and Syngas," *Process Safety Progress,* vol. 35, no. 3, pp. 237-251, 2017.

[23] J. Smith, A. Suo-Anttila, N. Philpott and S. Smith, "Prediction and Measurement of Multi-Tip Flare Ignition," Sheraton Maui, Hawaii - SepteSheraton Maui, Hawaii, September 26 –29 (2010).

[24] R. Said, A. Garo and R. Borghi, "Soot Formation Modeling for Turbulent Flames," *Combustion and Flame,* vol. 108, pp. 71-86, 1997.

[25] A. Suo-Anttila, K. Wagner and M. Greiner, "Analysis of Enclosure Fires Using the ISIS-3D CFD Engineering Analysis Code," in *12th International Conference on Nuclear Engineering*, Arlington, Virginia, April 25-29, 2004.

[26] J. Smith, R. Jackson, A. Suo-Anttila, K. Hefley, Z. Smith, D. Wade, D. Allen and S. Smith, "Radiation Effects on Surrounding Structures from Multi-Point Ground Flares," in *AFRC 2015 Industrial Combustion Symposium*, Historic Fort Douglas Officers Club University of Utah, Salt Lake City, Utah, September 9-11, 2015.